INL/RPT-23-71992
Revision 0

Advanced Gas Reactor Fuel Specification Technical Bases

March 2023

Paul A. Demkowicz
Douglas W. Marshall
Idaho National Laboratory

John D. Hunn
Oak Ridge National Laboratory

INL is a U.S. Department of Energy National Laboratory
operated by Battelle Energy Alliance, LLC

INL/EXT-23-71992
Revision 0

Advanced Gas Reactor Fuel Specification Technical Bases

Paul A. Demkowicz
Douglas W. Marshall
Idaho National Laboratory

John D. Hunn
Oak Ridge National Laboratory

March 2023

Idaho National Laboratory
Advanced Reactor Technologies
Idaho Falls, Idaho 83415

http://www.art.inl.gov

Prepared for the
U.S. Department of Energy
Office of Nuclear Energy
Under DOE Idaho Operations Office
Contract DE-AC07-05ID14517

Page intentionally left blank

INL ART Program

Advanced Gas Reactor Fuel Specification Bases

INL/EXT-23-71992
Revision 0

March 2023

Technical Reviewer:

David Petti

3/29/2023

David A. Petti
INL Emeritus Fellow

Date

Approved by:

Travis Mitchell

3/29/2023

Travis R. Mitchell
ART Project Manager

Date

Gerhard Strydom

3/29/23

Gerhard Strydom
ART-GCR National Technical Director

Date

Michelle Sharp

3/29/2023

Michelle T. Sharp
INL Quality Assurance

Date

ABSTRACT

The technical bases for the tristructural isotropic (TRISO) coated particle fuel specifications used by the Advanced Gas Reactor (AGR) program during its fabrication process development and fuel qualification efforts are provided based on historical high-temperature gas-cooled reactor (HTGR) fabrication experience in the U.S. and Germany and on improvements and insights gained during the AGR program execution. The technical bases are provided for specified properties of the kernel, the TRISO coating layers, the fuel particle, and fuel compact in terms of fabricability considerations, in-pile fuel performance, and fission product release under normal and off-normal conditions.

CONTENTS

FIGURES

TABLES

Page intentionally left blank

ACRONYMS

2-MGEM	two-modulator generalized ellipsometry microscope
ADUN	acid-deficient uranyl nitrate
AGR	Advanced Gas Reactor
AGR-1	first AGR irradiation test
AGR-2	second AGR irradiation test
AGR-3/4	third AGR irradiation test
AGR-5/6/7	fourth AGR irradiation test
ART	Advanced Reactor Technologies
ATR	Advanced Test Reactor
BAF_O	optical Bacon Anisotropy Factor
BWXT NOG	BWX Technologies Nuclear Operations Group
CO	carbon monoxide
CVD	chemical vapor deposition
DUF	dispersed uranium fraction
EKF	exposed kernel fraction
FIMA	fissions per initial metal atom
GA	General Atomics
GT-MHR	Gas Turbine Modular Helium Reactor
HMC	heavy metal contamination
HOBEG	Hochtemperaturreaktor-Brennelement GmbH
HRB	High Flux Isotope Reactor Removable Beryllium
HTGR	high-temperature gas-cooled reactor
INL	Idaho National Laboratory
IPyC	inner pyrolytic carbon (a.k.a. inner pyrocarbon) layer
LBL	leach-burn-leach
LL_M	lower range limit for the mean
LL_P	lower critical limit for the population
MHTGR	Modular High-Temperature Gas-Cooled Reactor
MTS	methyltrichlorosilane
NGNP	Next Generation Nuclear Plant
NPR	New Production Reactor
OPTAF	optical anisotropy factor
OPyC	outer pyrolytic carbon (a.k.a. outer pyrocarbon) layer

ORNL	Oak Ridge National Laboratory
PIE	post-irradiation examination
PyC	pyrolytic carbon (a.k.a. pyrocarbon)
QC	quality control
SiC	silicon carbide
SDF	SiC defective coating fraction
TRISO	tristructural isotropic
UCO	a mixed ceramic of UO_2 and UC_x phases, commonly referred to as “uranium oxycarbide”
UL_M	upper range limit for the mean
UL_P	upper critical limit for the population
UO_2	uranium dioxide

Advanced Gas Reactor Fuel Specification Technical Bases

1. INTRODUCTION

The Advanced Gas Reactor (AGR) irradiation experiment series was designed to re-establish the capability to manufacture tristructural isotropic (TRISO) nuclear fuel in the U.S. and to provide essential data to develop and qualify a fuel for a first-of-a-kind, high-temperature gas-cooled reactor (HTGR) and associated systems to generate electrical power and produce hydrogen or process heat. Fuel qualification is needed to support licensing, operation, and near-term deployment of an HTGR. Toward this objective, the Department of Energy (DOE) Advanced Gas Reactor Fuel Development and Qualification program (AGR program), which is currently part of the DOE Advanced Reactor Technologies (ART) program, led the development and fabrication of TRISO nuclear fuel at Oak Ridge National Laboratory (ORNL) and BWX Technologies Nuclear Operations Group (BWXT NOG) for a series of irradiation experiments in the Advanced Test Reactor (ATR) at the Idaho National Laboratory (INL) and post-irradiation examination (PIE) at INL and ORNL.

The fuel specification for the AGR Program was based initially on a specification developed by General Atomics (GA) and informed by GA's extensive experience in fuel fabrication and operating experience for Fort St. Vrain and follow-on fuel fabrication activities supporting irradiation campaigns for their modular HTGR designs (Scheffel and Tang 1989; Bresnik 1991; Munoz 1994). The GA specifications were impacted significantly by fabrication capabilities, with property ranges and critical limits based on experience from Fort St. Vrain, and in some cases were not directly tied to fuel performance.

The AGR program evolved and improved the earlier GA specifications based on several driving factors, including (1) programmatic decisions to transition to an overcoating process for compact fabrication, (2) development of new characterization methods for quality control (QC) and laboratory-scale fabrication at ORNL, (3) engineering-scale fabrication experience at BWXT NOG, and (4) computational modeling efforts at INL that could inform the specification of key values that impact fuel performance. Four irradiation tests were performed over the course of the AGR program; these tests were identified as AGR-1, AGR-2, AGR-3/4, and AGR-5/6/7 (Petti et al. 2010). Leading up to each irradiation test fuel fabrication campaign, the AGR fuel specification evolved to reflect insights from ongoing fuel performance modeling, feedback from the experimental irradiation campaigns, and changes in the reference reactor design and experimental needs for each irradiation test. The specifications and characterization methods discussed in this report are those established for the AGR-5/6/7 fuel (Marshall 2017), unless noted otherwise. The associated discussion of the technical bases also includes reference to earlier AGR program fuel specifications and to TRISO fuel development programs in the U.S. that predated the AGR program.

This report documents the technical bases for the fuel specifications developed for the AGR irradiation experiments to provide guidance for future specifications for coated particle fuel fabrication. The barriers against fission product release to the environment are (1) the fuel kernel, (2) the TRISO coatings, (3) the fuel body (i.e., the graphitic matrix) combined with the graphite blocks in the case of the prismatic reactor design, (4) the primary coolant pressure boundary, and (5) the reactor building. The efficiency of the first three barriers depends on the as-fabricated fuel quality and the operating envelope (including off-normal scenarios); the efficiency of the latter two barriers depends on the specific design of the reactor and reactor building. The ultimate fuel specifications will balance these barriers to achieve the desired "no public sheltering or evacuation response" beyond the exclusion area boundary for events within the emergency planning basis (Hanson 2001, 2009). Because of differences in reactor designs, performance requirements, and operating parameters, it is anticipated that fuel specifications for any

given reactor may differ from those used for fuel in the AGR-5/6/7 irradiation experiment. The information in this report is intended to provide supporting information for the development of fuel specifications for a specific reactor design.

2. DISCUSSION OF AGR-5/6/7 SPECIFIED PROPERTIES

HTGR fuel is composed of coated uranium ceramic fuel kernels, known as TRISO particle fuel. TRISO fuel is designed to contain most fission products during normal operation and accident conditions within the design and emergency planning bases. The particle is comprised of a spherical fuel kernel surrounded by a low-density pyrocarbon buffer layer, a high-density inner pyrocarbon layer (IPyC), a silicon carbide (SiC) layer, and a high-density outer pyrocarbon layer (OPyC). The TRISO particles are embedded in a matrix of graphite powders and a pyrolyzed phenolic resin binder—either as right-cylindrical rods that are inserted into hexagonal graphite fuel blocks for a "prismatic" reactor core or fuel spheres (referred to as pebbles) for a pebble-bed reactor. The focus of the AGR fuel development work has been to form cylindrical fuel compacts because the fuel particle packing fraction and service conditions of prismatic reactors generally envelope those for the pebble-bed design as well as operational requirements for the pebble-bed cores. This approach ensures that performance data are valid for either reactor design. Furthermore, the cylindrical compacts were a more suitable geometry for irradiation in the ATR.

The following sections discuss the specifications for the kernels, coating layers, and compacts used in the AGR program. There are a significant number of properties included in the specifications for this fuel system. Specified properties include both variable properties, which have measurable values that exhibit a distribution with sufficient normality, and attribute properties, which are treated as binary in nature (i.e., defective or non-defective). Variable property specifications are applied to the allowable range for the mean value and/or the population in the tails of the distribution (i.e., outside the specified critical limits of the property). Attribute properties are specified in terms of a maximum allowable defect fraction.

Except for a few variable properties for which measurement capabilities only support a point estimate, properties are evaluated for acceptance by analyzing representative samples taken from the product lot under evaluation and requiring that statistically determined confidence intervals for the specified criteria lay completely within the acceptable range. This approach establishes a margin to account for the statistical sampling and typically requires the evaluated lot to measurably exceed the specified criteria. If a property of the lot lies close to and within the allowable limit, then a large number of items from the lot must be sampled to reduce the width of the confidence interval enough to allow acceptance. The statistical methods used to determine the width of the confidence intervals are required by the AGR fuel specifications to apply a minimum confidence level of 95%. Mean ranges are typically evaluated using the Student's t-test and applying the one-tailed t-value associated with the number of measurements and the required minimum confidence to determine the confidence interval encompassing the mean. Critical limits are typically evaluated using a one-tailed k-factor associated with the number of measurements, allowable fraction outside the critical limit, and the required minimum confidence to determine the confidence interval encompassing the allowable population. These statistical methods also incorporate the standard deviation to account for the distribution of individual values for each measured component. Some measurements currently performed on bulk samples only obtain a value for the average and not the standard deviation of the discrete items in the sample. For these cases, the AGR fuel specification accommodated the comparison of a point estimate for the specified criteria to the specified range. Attribute properties are evaluated using mathematical probability methods, such as those based on a binomial or hypergeometric distribution. Details of how the fuel materials are statistically evaluated against the specified criteria can be found in the AGR program fuel specification, sampling plan, and statistical method reports (Marshall 2017; Einerson 2016, 2005; Kercher and Hunn 2005a).

The tables presented in this report contain (a) the specified properties, (b) the specified criteria for each property, and (c) a noncomprehensive list of the potential consequences of being outside the

specified criteria. As previously noted, the specified criteria are expected to vary with intended use such as reactor design or specifics of an irradiation test. In addition, the risk to fuel performance introduced by being outside the specified criteria will depend on multiple factors such as how much the fuel deviates from the specified criteria, how likely it is that deviation from a specified criteria will result in abnormal behavior, how significantly a resultant abnormal behavior impacts the overall fuel performance, and how sensitive the reactor design is to a specific type of fuel failure. These considerations determine whether the nonconforming lot can be used or must be discarded, as documented in a nonconformance report.

The history and reasoning behind the selection of the specified properties and determination of the specified criteria is discussed in the subsections following each table. The amount of available information and level of detail behind each specification varies. Some specifications are tied to stronger technical bases such as fuel performance calculations or previous experience in TRISO fuel irradiations. Others are based on experience and engineering judgement from historical TRISO fuel performance demonstrations worldwide. In some cases, systematic data does not exist for the extent of deleterious performance outside the specified criteria. However, the specifications are established so that the property limits are well within the range expected to result in acceptable fuel performance and to limit the population to very low fractions of fuel at the extreme ends of the distribution where fuel performance may begin to degrade.

In the tables below, specifications for the mean value ($\bar{x}$) of a property are presented with respect to the allowable lower limit for the mean ($LL_M \leq \bar{x}$), the allowable upper limit for the mean ($\bar{x} \leq UL_M$), or as a two-sided allowable range ($LL_M \leq \bar{x} \leq UL_M$). In the case of a two-sided allowable range, the AGR program usually targeted the value in the center of the range during fuel fabrication. Specifications for the dispersion of a property are presented in terms of the maximum allowable percentage of the population below the lower critical limit for the population ($\leq 1\% \leq LL_P$) or above the upper critical limit for the population ($\leq 1\% \geq UL_P$). Note that a specified tolerance limit of ≤1% of the population above the upper critical limit is equivalent to a requirement that statistical sampling must show at least 99% of the population is below the upper critical limit to the specified confidence level. Criteria for attribute properties are specified by the upper limit for the defect fraction (e.g., $\leq 1.0 \times 10^{-4}$). The AGR-5/6/7 specifications listed in the tables below required that statistical acceptance tests incorporated a minimum confidence level of 95%, except where noted.

All specifications apply to the lot from which the representative samples used for acceptance testing were drawn, except for the buffer and IPyC density, which were obtained from hot sampling during coating prior to deposition of the subsequent layer. The sampled lot could be a single process batch or a composite of multiple batches. The decision to perform acceptance testing on each process batch or on larger composites is dependent on a balance of efficiency and risk and should be informed by the process variability. It is often prudent to perform simple and quick analyses, such as kernel diameter and coating thickness, on every batch to prevent including a bad batch into a larger composite, which could spoil the larger composite and cause it to be rejected. Note that even if a bad batch does not cause a significant deviation in the mean value of a specified variable property, it may still lead to rejection if the presence of the batch causes the composite to fail the normality requirement of the applied statistical methods. Batch-level acceptance testing may also be required if multiple batches meet the specified criteria, but the composited batches will fail a normality test due to batch-to-batch variability.

2.1 Fuel Kernel

2.1.1 Kernel Purpose

Aside from its obvious function of supplying the fissile material for the fuel, the kernel is the initial substrate for the TRISO coating layers and serves as the primary retention component for most of the fission products generated during the irradiation of the fuel particle. As the initial substrate for the TRISO

coating process, the kernel's shape and uniformity of diameter and density can impact the quality and uniformity of the coated layers. Spherical shells are the ideal geometry for the TRISO coatings, and large deviations from spherical shape can increase the probability of coating failure during reactor operation and high-temperature excursions. Parameters impacting the fluidization and coating rate of kernels and particles in the coating chamber throughout the coating process are dependent on their size and mass. Tight distributions in the size and mass of the kernels in the coating charge can help obtain optimal coating conditions throughout the TRISO coating process. The chemical makeup of the kernel can impact the kernel performance. In the uranium carbide/uranium oxide (UCO) fuel kernel, metallic fission products form stable oxides and carbides that are mostly retained within the kernel. Uranium carbide acts as a getter for excess oxygen to prevent oxidation of the surrounding buffer layer, which would otherwise form CO that ultimately limits performance at higher burnup (Homan et al. 1977). Therefore, achieving an acceptable fraction of uranium oxide and uranium carbide is important. Additionally, excess silicide-forming metallic impurities in the kernel can add additional possibility for reaction with and degradation of the SiC layer structure.

2.1.2 Kernel Fabrication

The UCO kernels used in the AGR program were fabricated by BWXT NOG using an internal gelation sol gel process followed by carbothermic reduction to convert UO_3 and C powder contained in the gel spheres to $UO_{2-\partial}$ and UC_x (Barnes et al. 2008, Ebner 2005). In the as-fabricated kernels, a slightly substoichiometric uranium dioxide was thermodynamically favored and the uranium carbide formed during the carbothermic reduction process was present in two distinct phases of uranium monocarbide and substoichiometric uranium dicarbide (Kercher and Hunn 2005b, 2006). During coating and compacting, uranium monocarbide in the as-fabricated kernels converted to the more stable uranium dicarbide phase via reaction with carbon in the buffer layer at the process temperatures used for coating and during the 1800°C compact heat treatment (Hunn 2004a, Hunn et al. 2005).

2.1.3 Kernel Specifications

An overview of the UCO fuel kernel specifications is given in Table 1. The specification is applied to the as-fabricated kernel lot prior to riffling out material for coating. A more detailed discussion of each specification follows.

Table 1. As-fabricated AGR-5/6/7 UCO fuel kernel lot specifications.

Property	Specification	Possible Consequences
Diameter (μm)	$415 \leq \bar{x} \leq 435$ $\leq 1\% \leq 375$ $\leq 1\% \geq 475$	**Below LL_M or Above UL_M**—Deviation in U loading. Deviation from optimized coating process due to change average kernel diameter. **Above UL_P**—Significantly larger kernel/buffer volume ratio, and less volume for fission gases relative to kernel volume.
Aspect ratio	$\leq 10\% \geq 1.05$	**Above UL_P**—High aspect ratio of coated particles adds significant stress risers in coating layers.
Envelope density (g/cm^3)	$10.4 \leq \bar{x}$	**Below LL_M**—Increased friability/frangibility that could significantly increase kernel fracture during coating and lead to higher particle failure fractions as well as higher average and/or localized U contamination in the coating layers. Low U loading. Less fission product retention in the kernel.
Uranium fraction gU/g-kernel	$0.885 \leq \bar{x}$	**Below LL_M**—Could indicate excess carbon.
^{235}U enrichment (wt%) [a]	$15.4 \leq \bar{x} \leq 15.6$	**Below LL_M**—Low fissile loading, heat generation, and burnup. **Above UL_M**—High fissile loading and heat generation.

Property	Specification	Possible Consequences
C:U atom ratio	$0.30 \leq \bar{x} \leq 0.50$	**Below LL_M**—Higher CO pressure, kernel migration, and SiC corrosion; margin exists in terms of the carbide content at which deleterious behavior is expected. **Above UL_M**—Increased rare-earth fission product mobility.
O:U atom ratio	$1.30 \leq \bar{x} \leq 1.70$	**Below LL_M**—Excessive uranium carbide; could imply high impurities; high rare-earth mobility. **Above UL_M**—High oxygen content may deplete the uranium carbide phase faster than anticipated and generate CO during irradiation.
(C+O):U atom ratio	$\bar{x} \leq 2.0$	**Above UL_M**—Excess carbon resulting in lower density.
Microstructure [b]	Visual inspection for information only	Presence of noticeably low content of either phase in individual kernels indicates process nonuniformity that could impact overall performance.
Li, Na, Al, Cl, Ca, V, Cr, Mn, Fe, Co, Ni, Cu, and Zn (ppm-wt)	$\bar{x} \leq 100$ each	**Above UL_M**—Degradation of the SiC layer (metals) and U dispersion (Cl impurity). Increased parasitic neutron capture.
S and P (ppm-wt)	$\bar{x} \leq 1500$ each	**Above UL_M**—Detrimental to metallic components used in the reactor.

a. The U enrichment specified in this table is provided as an example and reflects the AGR-5/6/7 target value. The comments pertain to the consequence of deviating from the specified value and not to the establishment of the enrichment specification itself. U enrichment will be dependent on application (i.e., reactor core design).

b. The kernel microstructure specification calls for inspection of kernel cross sections and comparison to a visual standard for information purposes only to provide feedback on the presence of kernels with abnormally high or low carbide/oxide ratios.

2.1.4 Kernel Diameter

A mean diameter for each kernel in a random sample is determined using shadowgraph methods and automated image analysis. Historically, kernels with diameters from approximately 200–600 μm have been used in TRISO particle fuel types, with U enrichment typically varying for different kernel sizes. From a fuel performance perspective, the diameter is important because of its relationship with uranium loading at a given volumetric packing fraction in the final fuel form and because the relative capacity of the buffer layer to accommodate fission gases has an inverse relationship with the kernel/buffer volume ratio. Larger kernels require a lower volumetric particle packing fraction within the fuel form for a given uranium loading compared to smaller kernels (assuming the same coating thicknesses) but also result in a reduced void capacity within the buffer to contain fission gases for the same layer thickness. From a fuel fabrication perspective, larger diameter kernels have better fluidization characteristics than smaller kernels, which allows for somewhat larger kernel mass charges to the coater and improved fabrication economics.

The AGR-5/6/7 fuel specification kept the 425 μm nominal kernel diameter size for consistency with the AGR-2 experiment and the single-particle core design studies performed for NGNP[*], and to enable a

[*] Previous GA HTGR designs used a fissile-fertile two-particle system. The 350 μm kernel used for AGR-1 was the fissile particle for the GA MHTGR design. Subsequently, a large effort was devoted to establishing a neutronically equivalent single particle design which resulted in a 425 μm kernel. The original effort prescribed an enrichment of 14–14.5% but this was subsequently increased to 15.5% to accommodate margin since the neutronic studies were largely conceptual at that stage of the project.

higher uranium loading at the desired particle volumetric packing fractions relative to the 350 μm nominal fissile kernel of the Modular High-Temperature Gas-Cooled Reactor (MHTGR) design (General Atomics 2009). The lower critical limit on the diameter ensures satisfactory uranium loading and the upper critical limit reduces the probability of excessive pressure buildup during irradiation from the reduction in relative buffer capacity (Petti et al. 2004). The critical limits also ensure a sufficiently narrow distribution of kernel sizes for coating and handling operations.

2.1.5 Kernel Density

Average kernel envelope density is measured by weighing several random samples consisting of thousands of kernels each and determining the total envelope volume of the kernels in each sample with a mercury porosimeter. While this method accurately determines the average envelope density, it does not yield information on the dispersion of individual kernel densities in the sampled population. The envelope density of the kernel needs to be near the theoretical density to provide a rugged, infrangible substrate for coating, limit the fission gas release from the kernel during irradiation, ensure acceptable uranium loading for fuel particles, and decrease the required packing fraction for fuel particles and the potential for manufacturing defects during fuel compact fabrication (Adams et al. 1992).

Fission gas retention in failed coated particles with uranium dioxide (UO_2) kernels with an 80% theoretical density released an order of magnitude more krypton and xenon than failed particles with kernels that were initially 97% dense (Pointud and Chenebault, 1977). Thus, high envelope density has been shown to minimize fission gas release.

2.1.6 Kernel Aspect Ratio

The diameter aspect ratio is characterized by measuring the ratio of the maximum and minimum diameter in conjunction with the shadowgraph image analysis used for measuring average kernel diameter. This aspect ratio is used as a metric for sphericity in the AGR fuel specifications. Deviation from a spherical shape results in non-uniform stresses in the TRISO layers, particularly in the SiC layer, and may compromise in-pile fuel particle performance (Miller, Petti, and Maki 2004) or performance during safety testing (Hunn et al. 2014). Coatings are applied by chemical vapor deposition in a spouted bed, which is characterized by an axial spout of gases and entrained particles rising through the particle bed, a fountain of disengaged particles falling back to the bed surface, and a subsiding annular fluidized bed of loosely packed particles. Spherical particles have no preferred orientation in the annular fluidized bed, but significantly aspherical particles do, which inhibits particle rotation and uniform coating deposition. Coating gases not only pass up through the spout, but also percolate through the annular fluidized bed, depositing materials on the exposed particle surfaces. In addition, the shape of the substrate impacts the coating rate, with surface areas of higher positive curvature receiving thicker deposits because of the higher solid angle presented to the coating gases.

Experience shows that the aspect ratio can be exacerbated as each successive coating layer is deposited and that achieving spherical TRISO particles depends on starting with spherical kernels. The gas turbine modular helium reactor (GT-MHR) and MHTGR fuel specifications developed by GA did not include values for kernel aspect ratio (Barnes 2006). In the AGR program, this specification is imposed to improve the probability for satisfactory sphericity of the SiC layer and to minimize friability that has been observed to be associated with protruding surface features of some UCO kernels (Hunn 2004a). These considerations led to the AGR specification that ≤10% of the kernels have an aspect ratio ≥1.05. Aspect ratio measurements of 100 randomly selected AGR-5/6/7 fuel kernels indicated that the kernel lot could have passed a more stringent critical limit specification of ≤10% of the kernels exceeding an aspect ratio of 1.020 (Marshall 2020). This finding indicates that the kernel lot was well within the specified limit of ≤10% ≥1.05. Additional discussion on the coated particle aspect ratio specification is provided in Section 2.4.6.

The diameter aspect ratio is best applied to oblate spheroids, which present a maximum aspect ratio in the shape of an ellipse, because the entire perimeter of an ellipse is defined by the minimum and maximum axes. In a study of German UO_2 kernels produced by external gelation, aspherical kernels generally presented elliptical shadowgraph projections that could be well described by their minimum and maximum diameters (Hunn 2004b). While UCO kernels produced under the AGR program generally exhibited good sphericity, kernels with abnormal asphericity tended to exhibit localized areas of high curvature due to surface nodules or fractures (Hunn 2004a; Marshall 2020). These shapes are not well characterized by aspect ratio. Automated image analysis used for analyzing kernel shadowgraphs supports an alternate metric for classifying asphericity based on the maximum and minimum local curvature, which highlights high curvature regions at the edge of fractures and the apexes of protrusions and also highlights low curvatures along the flats of facets (Price et al. 2006). These metrics were applied to identify and characterize aspherical UCO kernels from the kernel composite used in the AGR-1 irradiation experiment (Kercher and Hunn 2005b). Higher curvature regions on the kernel surface are more susceptible to erosion during fluidization in the coating furnace and both flat and sharp edges tend to propagate to form aspherical coatings. Therefore, there may be value in classifying shape with a metric sensitive to these features. However, additional effort would be required to establish criteria for specifying unacceptable asphericity using these metrics.

2.1.7 Kernel Enrichment

Average kernel enrichment is measured using several random samples consisting of thousands of kernels each. The kernels are dissolved in acid, and aliquots of the acid are analyzed to determine the uranium isotope mass ratios using standard analytical mass spectrometry methods. While this analysis only determines the mean enrichment in the kernel lot, a broad dispersion in enrichment is not expected in a well-controlled kernel fabrication process because enrichment is first determined in the acid-deficient uranyl nitrate (ADUN) solution and the sol-gel process will not change the enrichment. If critical limits for the enrichment need to be specified, they can be determined from measurement of the ADUN enrichment prior to each kernel forming run. The 15.5% uranium enrichment was expected to bound the enrichment of first core HTGR fuel and to be representative of the reload fuel for the Next Generation Nuclear Plant (NGNP) design (Hanson 2009, General Atomics 2010). The specified enrichment was experiment- and reactor design-specific and ranged from 14.0%–19.8% in the UCO fuel irradiated by the AGR program.

2.1.8 UCO Kernel Phase Fractions

The UCO kernel phase fractions are key to ensuring the presence of appropriate quantities of uranium oxide and uranium carbide throughout the maximum expected burnup of the fuel (Homan et al. 1977; McMurray et al. 2017). The presence of an oxide phase contributes significantly to the chemical stability of metallic fission products within the kernel volume. The presence of the carbide phases in UCO limits the oxygen activity in the kernel as fission progresses, which minimizes the quantity of carbon monoxide (CO) generated by oxygen reacting with the carbonaceous buffer layer. The reduction in CO generation reduces the internal pressure, prevents kernel migration into the buffer (the “amoeba effect”), and limits the CO reaction with SiC to form silicon monoxide (SiO), all of which reduce the likelihood of in-pile particle failures relative to kernels composed solely of UO_2 (Maki et al. 2007; Verfondern, Nabielek, and Kendall 2007). Ideally, uranium carbide content should be kept as low as is feasible for a given target burnup to maximize the fraction of the oxide phase without generating excess CO.

Early U.S. fuel specifications for UCO kernels relied on specifying the atomic ratios of O:U and C:U to control UCO phase fractions and this approach was adopted by the AGR program. Average mass fractions of U, C, and O are determined by analyzing random samples consisting of thousands of kernels each. The average mass fraction of U is measured by dissolving kernels in acid and measuring uranium

content with Davies-Gray titration and mass spectrometry. The average mass fractions of C and O are determined with combustion analyzers.

In general, the C:U specification ensures a limited CO production and an inhibited kernel migration during irradiation. The low end of the C:U range is specified to ensure that there are sufficient quantities of carbide throughout the irradiation to limit the oxygen potential in the kernel that would otherwise increase from UO_2 fission, thereby limiting the reaction of the kernel with the buffer to form CO. The lower bound on the mean O:U is specified to ensure that there is sufficient oxide phase in the kernel so that most of the rare-earth fission products form stable, immobile oxides and limit the amount of metal carbides, which can result in higher mobility of the fission products. The immobilization of fission products as oxides applies especially to rare-earth metal fission products (including La, Ce, and Nd), which have been found to corrode the SiC layer in TRISO particles with carbide kernels (Homan et al. 1977).

A mean O:U between 1.30 and 1.70 was specified in the GT-MHR fuel specification (Munoz 1994). The AGR specifications all maintained this range for the mean O:U ratio. Ignoring the expected slight substoichiometry of the uranium dioxide component, this corresponds to 65%–85% of the uranium present as UO_2 and 15%–35% of the uranium present in some other form (presumably uranium carbide). A mean C:U between 0.30 and 0.70 was specified in the GT-MHR fuel specification (Munoz 1994). All the AGR specifications retained the lower limit of 0.3 on the mean C:U ratio. This lower limit ensures a mean uranium carbide content of at least 15%. Scheffel and Tang (1989) identified a UC_2 content of 15% as an optimum phase composition at the start of irradiation. Thermodynamic models have indicated that 5.1%–5.5% uranium carbide in as-fabricated 15.5% enriched UCO kernels is sufficient to ensure uranium carbide presence is maintained throughout irradiation up to 16.1% burnup (McMurray et al. 2017).

The upper limit for a mean C:U ratio of 0.70 used in the GT-MHR specification is consistent with the lower bound of 1.30 for O:U if all uranium is present as either UO_2 or UC_2, which appears to be an assumption used in the selection of the specified O:U and C:U ranges (Scheffel and Tang 1989). The AGR-1 specification retained this upper bound of 0.70 for mean C:U ratio. The AGR-2 and AGR-5/6/7 specifications called for a mean C:U ratio between 0.30 and 0.50. The lower upper limit on the mean of 0.50 was consistent with process limitations at the time, in which a significant fraction of the uranium carbide was present in the monocarbide phase (Ebner 2005).

The presence of free carbon was observed in UCO kernels fabricated at BWXT during early AGR program development efforts (Ebner 2004). As a result, an upper limit on the mean (C+O):U of $\bar{x} \leq 2.0$ was added in the second revision of the AGR-1 fuel specification (Barnes 2005) to reject kernels that clearly contained free carbon. In kernels in which all of the uranium oxide phase is UO_2 and all of the uranium carbide phase is UC_2, a (C+O):U ratio above 2 indicates the presence of free carbon in addition to that in the uranium carbide. Note that free carbon may still be present for (C+O):U ≤ 2.0 if monocarbide is present.

The specification on the mean uranium fraction of $\bar{x} \geq 0.885$ gU/g-kernel is essentially redundant to the specification of (C+O):U ≤ 2.0 in conjunction with the specified ranges for O:U and C:U. The minimum uranium fraction associated with C:U = 0.30 and O:U = 1.70 for a UO_2-UC_2 stoichiometric kernel is 0.8854. Stoichiometric UO_2-UC_2 kernels with O:U < 1.70 have uranium fractions >0.8854. However, the uranium fraction is <0.8854 for UO_2-UC_2 kernels with extra free carbon, such that (C+O):U > 2.0. For example, the uranium fraction associated with C:U = 0.32 and O:U = 1.70 for a kernel of UO_2 and UC_2 plus free carbon is 0.8846.

2.1.9 Kernel Microstructure

The O:U and C:U kernel stoichiometry measurements used for acceptance testing of AGR irradiation test fuel do not provide information on kernel-to-kernel variation in the ratio of oxide and carbide phases because they are performed on bulk samples. However, if the process can produce kernels that deviate

significantly from the mean stoichiometry specification, it could result in kernels composed of nearly 100% oxide or 100% carbide phase. Kernels with close to 100% oxide phase would have negligible amounts of uranium carbide phase to control oxygen potential in the kernel, which would result in the production of CO gas that could impact particle performance. Kernels with close to 100% carbide phase would exhibit greater chemical attack of the SiC by rare-earth fission products typically retained as oxides in kernels with UO_2 (Homan et al. 1977). Early U.S. fuel specifications included critical limits on the C:U ratio of ≤1% ≤0.20 and ≤1% ≥0.80 to limit the population of kernels significantly outside the specified range for the mean. Because a feasible quantitative UCO kernel chemistry analysis method with individual kernel resolution was not yet available but is needed for statistical acceptance tests associated with a critical limit, the AGR-2 and AGR-5/6/7 fuel specifications replaced the critical limit specification with a requirement to cross section kernels from each batch and inspect for evidence of the presence of both oxide and carbide phases.

The visual standard for kernel microstructure used in the AGR-5/6/7 specification shows evidence of interspersed oxide and carbide phases within the kernel (Figure 1). Photomicrographs of sectioned kernels provided documentation of the phase distribution. During AGR-1 kernel fabrication and subsequent kernel development, considerable effort went into improving phase distribution within UCO kernels by improving carbon dispersion during broth preparation (Ebner 2005). This visual inspection for information only was required in the AGR program fuel specification to provide a qualitative assessment on the kernel-to-kernel variation in carbide and oxide phases in order to evaluate the success of the improved broth preparation and carbothermic reduction processes and identify aberrations that could potentially impact fuel performance. Post-AGR-5/6/7 development efforts have produced a method for measuring the UCO kernel phase fractions in individual kernels that provide an option for inclusion of critical limit criteria in future fuel specifications (Helmreich et al. 2020a).

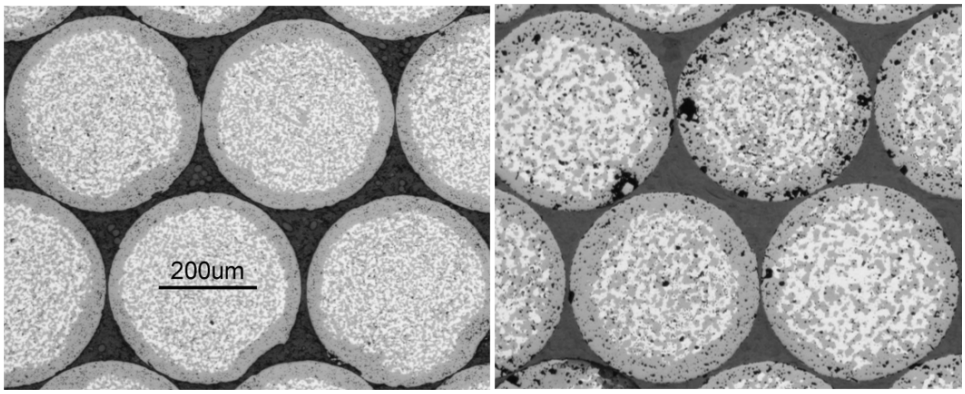

Figure 1. Examples of acceptably interspersed oxide (gray) and carbide (white) phases. Structure on the left is preferred (images from Marshall 2017).

2.1.10 Kernel Impurities

The average mass fraction of each specified kernel impurity is measured in several random samples consisting of thousands of kernels dissolved in acid, which are then analyzed with standard mass spectrometry methods. The AGR specifications for kernel impurities were established using the same technical bases used for specifications developed by GA for fuel fabrication (Scheffel and Tang 1989; Adams et al. 1992). The specified impurities were selected because of the likelihood of their inclusion in the fuel kernels (a result of the fabrication process, impurities in the associated feedstock, or the presence of external contamination sources) and their potential to negatively impact fuel performance. The specified impurities do not represent a comprehensive list of all detrimental foreign contaminants. Changes to any of the contributing factors may require the addition of other impurities detrimental to fuel performance to the specification.

Metals commonly found in the apparatus used for fuel manufacture (i.e., V, Cr, Mn, Fe, Co, Ni, Cu Zn, and Al), are included in the specification. Many of these may readily react with SiC to form silicides in a temperature range consistent with HTGR operating and accident conditions, thereby degrading the integrity of the layer. The ≤100 ppm-wt critical limit for Fe, Cr, Co, Ni, and Mn is based on past data from the DOE HTGR program that studied Fe migration and particle failure as a function of the level of measured iron impurities in the fuel. A kernel impurity content of 237 ppm-wt Fe was associated with observable Fe migration to the SiC layer in a thermal gradient, while particles with <100 ppm-wt Fe impurities in the kernels showed acceptable behavior (Scheffel and Tang 1989). Irradiation data revealed that particles with an equivalent of ~1000 ppm Fe in the kernel exhibited particle failure from Fe reaction with SiC, whereas particles with equivalent Fe in the kernel of less than ~500 ppm exhibited no failure. As Cr, Co, Ni, and Mn behave similarly to Fe with respect to SiC reaction, a limit of ≤100 ppm-wt was placed on each of these transition metals in the NP-MHTGR specification (Adams et al. 1992) so that the total concentration could not exceed 500 ppm.

The ≤100 ppm critical limit for Cl in the earlier DOE HTGR program was based on the need to reduce transport of uranium from the kernel, which could accelerate fission metal attack of the SiC layer. The ≤100 ppm limit for Na and Ca was based on the propensity of these elements to disrupt the SiC crystal lattice and degrade the fission product retention characteristics (Adams et al. 1992). The Cl, Na, and Ca impurity specifications were also based on previous successful irradiation tests for kernels meeting this specification. Previous fuel specifications also included either specific limits on the individual elements Li, Al, Cu, Zn, and V or included them in a general limit for total impurities with a limit of typically ≥1000 ppm, depending on the specification (Adams et al. 1992; Munoz 1994; Tang 1989). The AGR program adopted a conservative limit of ≤100 ppm for these elements individually.

A comprehensive dataset correlating individual impurity levels with SiC degradation and failure is not available, but these limits are established, in part, based on past irradiation experiments of fuel using kernels meeting these specifications (Petti et al. 2004). Analyses of AGR-1 (lot G73D-20-69302) and AGR-2 (lot G73I-14-69307) kernels showed that these impurities were below detection limits, which ranged from 5 ppm for Co to 50 ppm for Ca, Cr, Fe, Na, Ni, V, and Zn.

While most of the specified impurities can be controlled by selecting low-impurity feedstock and mitigating the introduction of impurities during processing, sulfur and phosphorus may be inherent constituents of the chemicals used in the sol gel process. Therefore, these elements are expected to be present at higher levels in the final kernel product. The AGR fuel specification limit of ≤1,500 ppm-wt for sulfur and phosphorus is based on engineering judgement and a previous fuel specification that had a limit of 5,000 ppm for the sum of all kernel impurities (Adams et al. 1992). The specified limit is higher for these impurities because they have negligible impact on the SiC, though they may be detrimental to metallic components used in the reactor. In the AGR kernel fabrication process, a sulfur-containing dispersant (later replaced by a sulfur-containing surface modified carbon) was used as a feedstock. The concentration of sulfur in sintered kernels was typically 590–620 ppm when the dispersant was used and 400–480 ppm when the surface modified carbon was used. The AGR-1 (kernel lot G73D-20-69302) and AGR-2 (kernel lot G73I-14-69307) kernels had 615 ppm and 373 ppm sulfur, respectively. Phosphorus was below the detection level (<30 ppm) in both cases. The kernel batches composing kernel lot G72R-16-69317, which were used in the AGR-5/6/7 experiments, had measured sulfur values from 240 to 314 ppm and phosphorous assayed at or below the detection limit of 25 ppm.

2.2 Buffer Layer

2.2.1 Buffer Purpose

The buffer layer protects subsequent coating layers by absorbing the kinetic energy of fission fragments ejected from the kernel during a fission event and providing void space for gaseous fission products to accumulate without incurring excessive internal pressures (Kugeler 2017). The buffer also

accommodates kernel swelling through shrinkage and densification, thus avoiding a buildup of spherical hoop stresses in the outer layers. Subsequent coating layers could be damaged during irradiation by physical stresses and chemical attack if the buffer layer was deficient or absent. The buffer also retards the migration of non-gaseous fission products by reacting with some of them to form carbides and by providing a tortuous migration path. PIE of TRISO particles has shown that intact buffer shells may reduce kernel swelling (Ploger et al. 2012; Ploger et al. 2014; Bower et al. 2017).

2.2.2 Buffer Deposition

All coating layers in the AGR-5/6/7 coated particles were deposited using a fluidized bed chemical vapor deposition (CVD) coating system with a 150-mm-diameter coating chamber. The buffer layer was deposited on the kernels using CVD of carbon produced by the thermolysis of acetylene in a pulsatory spouted particle bed at about 1420°C. Acetylene was diluted with argon (60:40) and injected into the bed where the gases are heated by the bed particles to the point of acetylene decomposition, which is highly exothermic and causes the bed temperature to rise in excess of 100°C during the course of the buffer deposition. Acetylene decomposes to form hydrogen gas and carbon in parallel homogeneous and heterogeneous nucleation pathways. The resulting porous carbon deposit accumulates at an average radial rate of ~18 μm/min and has a density near 1.0 g/cm^3.

2.2.3 Buffer Specifications

Buffer layer specifications are shown in Table 2.

Table 2. Buffer layer specifications for the TRISO particle lot.

Property	Specification	Possible Consequence
Thickness (μm)	$95 \leq \bar{x} \leq 115$ $\leq 1\% \leq 58$	**Below LL_P**—Higher probability for pressure vessel failure of SiC.
Envelope density (g/cm^3) [a]	$0.85 \leq \bar{x} \leq 1.15$	**Below LL_M**—Higher shrinkage during irradiation, resulting in a larger buffer-IPyC gap. Insufficient mechanical strength during IPyC deposition. **Above UL_M**—Insufficient void volume to accommodate fission gas and kernel swelling.

a. Mean buffer envelope density is determined using a point estimate from hot samples removed between the buffer and IPyC deposition, as described in Section 2.2.5, and may be pooled from multiple coating runs.

2.2.4 Buffer Thickness

A mean thickness for each buffer layer in a random sample of TRISO-coated particles is determined by cross sectioning and polishing the particles to near midplane and analyzing optical micrographs of the polished cross sections with automated image analysis. The required buffer layer thickness is driven by the need to attenuate fission product recoil and provide sufficient volume, in conjunction with the porous, low-density structure, to accommodate gases from fission and chemical reactions as well as kernel swelling. The quantity of gas that must be contained and the degree of kernel swelling are functions of the kernel mass and density, kernel chemistry, and the design basis burnup. Prismatic reactor designs often have higher burnup goals than comparable pebble-bed designs and may require thicker buffers for a given kernel diameter. The coated particle for the German MODUL reactor design had a buffer thickness specification centered around 100 μm (covering a 500-μm UO_2 kernel) and target peak burnup of approximately 10% fissions per initial metal atom (FIMA) (Kania et al. 2013). Considering the ratio of kernel and buffer volumes, the equivalent buffer thickness for HTGR fuel with a 425-μm kernel, 15.5% enrichment, and a peak burnup target of 16% FIMA would be approximately 110 μm if the kernel were

also made entirely of UO_2. The uranium carbide phases in the UCO kernel greatly reduce carbon monoxide generation during irradiation, which keeps internal pressures low, so that a 100 µm buffer thickness is satisfactory with densities near 1.0 g/cc. The AGR-5/6/7 TRISO-coated UCO particles (425-µm diameter kernel, 15.5 wt% enrichment) were modeled with PARFUME (Skerjanc et al. 2016). It was determined that the probability of SiC failure follows a power law relationship with buffer thickness. With a 100-µm-thick buffer layer, the SiC failure probability was approximately 7×10^{-7}.

2.2.5 Buffer Density

The average buffer envelope density is measured by weighing random samples consisting of thousands of buffer-coated kernels, determining the total envelope volume of the buffer-coated kernels in the sample using a mercury porosimeter, dividing by the number of buffer-coated kernels in the sample to get average mass and volume per particle, and using previously measured values for average mass and volume of the kernels to determine the buffer density, as described in the data acquisition method (Hunn 2006). While this method accurately determines the average buffer density, it does not yield information on the dispersion of individual buffer densities in the sampled population.

The buffer density is a compromise between providing (1) sufficient internal volume to accommodate CO and fission products that are gases at operating and accident temperatures, (2) sufficient strength to resist significant damage due to interparticle forces during fabrication, and (3) a low bond strength with the IPyC layer. PIE of AGR-1 particles has shown instances where buffer shrinkage has stressed the IPyC layer to the point of failure, pulled the IPyC away from the silicon carbide layer, and curled the IPyC layer inward at the breaks. This buffer and IPyC layer behavior is associated with damage to the SiC layer such as the tangential tears in the SiC layer seen in Figure 2.

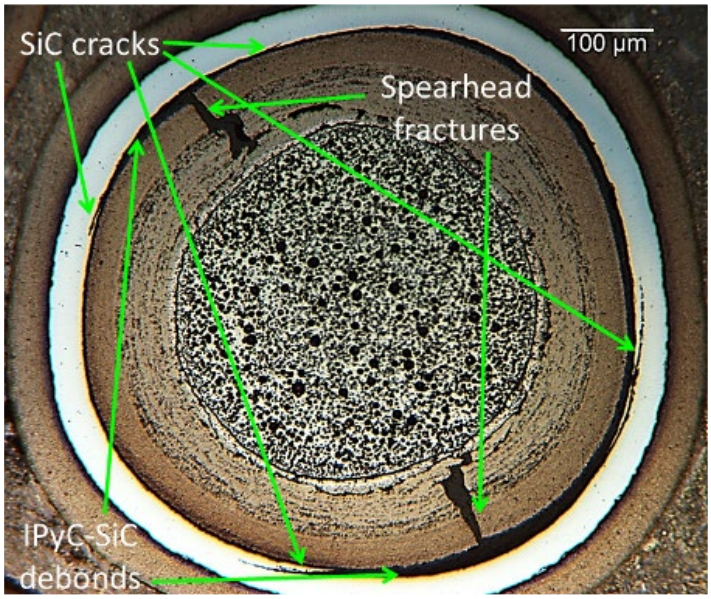

Figure 2. Damaged IPyC and SiC layers from buffer shrinkage in irradiated AGR-1 Variant 1 particle (image from Demkowicz et al. 2015).

Separation of the buffer from the IPyC layer was the dominant coating morphology in both the AGR-1 and AGR-2 irradiated particles examined in cross section. In addition, the fraction of AGR-2 particles exhibiting tears or cracks in the IPyC layer related to buffer-IPyC interaction was less than that of AGR-1 particles. It is hypothesized that this observation is a result of a weaker buffer-IPyC interface in the AGR-2 particles, which facilitates separation of the two layers and reduces the ability of the shrinking buffer layer to exert sufficient stress on the IPyC layer to cause tears. Observation of numerous irradiated

particles from AGR-1 and AGR-2 show that the detachment at the buffer-IPyC interface occurs via circumferential tearing of the buffer layer, which allows the bulk of the buffer to shrink away from the relatively fixed IPyC surface and leaves a thin layer of buffer remaining at the interface (Demkowicz et al. 2015; Stempien et al. 2021). This behavior may be related to either the presence of closed porosity bands in the buffer close to the IPyC presenting a perforated layer prone to tearing or to the extent of open porosity at the buffer surface affecting the depth of IPyC penetration in the buffer-IPyC interface region.

It is thought that particle-particle impacts during the transition from buffer deposition to IPyC deposition temperatures may densify the outer surface of the buffer and close some of the exposed pores. This surface densification, which does not appreciably impact the average buffer density, may decrease the bond strength between the buffer and the IPyC. During a parametric study of the relationships between the coating process and IPyC layer properties early in the AGR program (Lowden et al. 2005), difficulty in mechanically separating the IPyC layers from the underlying buffer was solved by extending the time that buffer-coated particles were fluidized in argon between the end of the buffer deposition and the start of the IPyC deposition. This extended inert gas fluidization increased the probability of IPyC separation during particle cracking. AGR-2 and AGR-5/6/7 particles were coated in an engineering-scale coater that inherently had a longer inert gas fluidization period compared to the lab-scale coater used for AGR-1 because of the longer time required to cool the larger engineering-scale coating chamber from the buffer deposition temperature to the IPyC deposition temperature. This may explain the different buffer-IPyC interface behavior observed between AGR-1 and AGR-2.

2.3 Inner Pyrocarbon Layer

2.3.1 IPyC Purpose

The IPyC layer provides a barrier against the infiltration of chlorine compounds generated during SiC deposition that react with the uranium in the fuel kernel and acts as a barrier to carbon monoxide gas and fission products that could reach the SiC layer and cause deleterious corrosion during operation. The IPyC also counteracts the stress on the SiC layer from internal particle pressurization during operation by shrinking under irradiation and inducing a compressive load on the SiC layer when the IPyC-SiC bond remains intact.

2.3.2 IPyC Deposition

The IPyC layer was deposited using CVD by the thermolysis of acetylene and propylene at about 1310°C in a pulsatory spouted bed (Marshall 2020). The acetylene and propylene coating gases were diluted with argon (16.2 : 13.8 : 70) upon injection into the bed. The coating gases decompose into hydrogen, carbon, and minor hydrocarbons in parallel homogeneous and heterogeneous nucleation pathways, resulting in a high-density pyrolytic carbon deposit (~1.9 g/cm^3) with predominantly randomly oriented graphene crystallites. The random orientation of the crystallites provides for the highly isotropic thermal and physical properties of the pyrocarbon layer. The IPyC layer is deposited at an average radial rate of approximately 3.0 μm/min.

2.3.3 IPyC Specifications

The IPyC layer specifications are given in Table 3.

Table 3. Inner pyrocarbon layer specifications for the TRISO particle lot.

Property	Specification	Possible Consequence
Thickness (μm)	$36 \leq \bar{x} \leq 44$ $\leq 1\% \leq 30$ $\leq 1\% \geq 52$	**Below LL_P**—Higher permeability that could increase defective IPyC fraction. **Above UL_P** – Increased stress in the IPyC layer during operation that can increase the probability of IPyC cracking, which can increase probability of SiC failure.
Sink-float density (g/cm^3) [a]	$1.85 \leq \bar{x} \leq 1.95$ $\leq 1\% \leq 1.80$ $\leq 1\% \geq 2.00$	**Below LL_P**—Higher permeability that could increase defective IPyC fraction; increased SiC degradation by fission products. Higher shrinkage; lower fission product retention. **Above UL_P**—Density correlates with anisotropy so that densities exceeding the critical limit will result in excessive anisotropy and poor coating performance.
Diattenuation	$\bar{x} \leq 0.0170$ $\leq 1\% \geq 0.0242$	**Above UL_P**—Anisotropic shrinkage inducing stress in IPyC and SiC layers.
Defective IPyC fraction [b]	$\leq 1.0 \times 10^{-4}$	**Above Limit**—Increased fraction of SiC defects created during fabrication and increased level of fission product degradation of the SiC layer during operation.

a. IPyC density specifications are specific to density measured by sink-float technique and measured on samples extracted from the coater before SiC deposition.

b. Defective IPyC fraction is measured in particles after heat treatment to simulate thermal conditions particles experience as part of compact fabrication, which enhances Cl leaching of uranium from kernel. Defective particles are defined based on intensity of uranium visible in a radiograph outside the kernel compared to a visual standard.

2.3.4 IPyC Thickness

A mean thickness for each IPyC layer in a random sample of TRISO-coated particles is determined by cross sectioning the particles to near midplane and analyzing optical micrographs of the polished cross sections with automated image analysis. IPyC thickness specifications are based on the need to establish a lower limit to avoid particle defects during fabrication and an upper limit to avoid excessive stress in the coating layers during operation, which can lead to particle failure. To be effective, the IPyC layer must have a sufficient thickness to preclude connected pores from penetrating the full thickness of the layer. Increased IPyC permeability is a concern during fuel fabrication, where chlorine-based byproducts generated during SiC layer deposition can reach the kernel and disperse uranium throughout the buffer layer or beyond. Such particles are identified as having a defective IPyC layer, which impacts fuel performance (see Section 2.3.7).

Another factor that contributes to the minimum practical IPyC thickness is the role interstitching at the IPyC-SiC interface plays in generating a strong, intimate bond between these two layers. While connected porosity throughout the IPyC layer is undesirable, open porosity at the IPyC surface allows SiC infiltration into the IPyC structure at the beginning of the SiC deposition. The resultant interstitching of the two layers minimizes debonding of the IPyC from the SiC during irradiation, which appears to reduce the probability of SiC failure (Petti et al. 2004). Therefore, ideal IPyC must have an overall low permeability through the layer while still having a small region at the outer surface (a few micrometers) of connected porosity.

German fuel specifications in the 1980s called for an IPyC layer thickness of 30–50 μm, with the fabricated mean value falling in the middle of this range (39 μm; Heit et al. 1985). In the U.S. HTGR program, it was recognized based on process development studies that >18 μm thickness of IPyC with an envelope density ≥1.85 g/cm^3 was needed to provide adequate protection to the kernel during fabrication (Scheffel and Tang 1989). This resulted in a lower critical limit of 20 μm in fuel product specifications of the time (Munoz 1994). The AGR program subsequently established a critical limit of 30 μm for the AGR series of experiments on the basis of preventing Cl permeation of the layer during fabrication (Petti et al. 2004) and in recognition of the good performance of TRISO fuel in the German irradiation experiments.

The IPyC layer plays an important role in the thermomechanical behavior of the coating layers, with irradiation shrinkage of the layer imparting a beneficial compressive stress onto the SiC layer. However, as the IPyC layer thickness increases, the stress in the layer also increases. Consequently, the probability of IPyC layer cracking leading to SiC failure also increases, which threatens particle integrity. The U.S. GT-MHR fuel specification called for an upper critical limit of 50 μm for IPyC thickness (Munoz 1994). Computational modeling of particle performance led the AGR program to establish an upper critical limit of 56 μm (Petti et al. 2004). Subsequent modeling efforts led to a revised upper critical limit of 52 μm based on the increase in SiC failure probability with increasing IPyC thickness (Skerjanc et al. 2016).

2.3.5 IPyC Density

Sink-float density of each IPyC fragment in a random sample of fragments taken from a sample of IPyC/buffer-coated particles is determined by measuring its neutral buoyancy position in a linear-gradient density column. Density and structural anisotropy in CVD IPyC are inextricably connected; both are dependent on the nature of the carbon crystallite nucleation (homogeneous vs. heterogeneous) and deposition. A high deposition temperature shifts thermolysis toward homogenous nucleation, small crystallite sizes, and random crystallite orientation, which yields a lower pyrocarbon density and lower structural anisotropy. Conversely, low deposition temperatures shift thermolysis toward heterogeneous mechanisms, larger crystallites sizes, and a greater degree of crystallite orientation, yielding a higher pyrocarbon density and higher structural anisotropy. Early AGR program parametric studies of IPyC deposition in a fluidized bed showed that IPyC density primarily scaled inversely with coating temperatures between 1225°C and 1325°C, while diattenuation (which relates to structural anisotropy, as discussed in Section 2.3.6) scaled inversely with both temperature and coating gas fraction (Lowden et al. 2005).

An adequate pyrocarbon density is needed to protect the kernel from exposure to chlorine compounds generated during the SiC deposition that can result in uranium dispersion and its associated impacts to fuel performance (see Section 2.3.7). The permeability of the IPyC is thought to be sufficiently low when the mean IPyC density exceeds 1.85 g/cm^3 (Scheffel and Tang 1989). The upper limit of 1.95 g/cm^3 for the mean IPyC density was originally imposed by Scheffel and Tang (1989) because it represented the limit of contemporary irradiation testing experience. A high-density pyrocarbon may be too brittle and the level of shrinkage too limited to impose adequate compressive forces on the SiC shell. The upper critical limit for IPyC density is set at approximately 90% of the theoretical density.

2.3.6 IPyC Anisotropy

Historical data have shown that a high degree of preferred orientation of the graphitic crystallites within a pyrocarbon (PyC) layer can lead to failure of the PyC layer during irradiation due to anisotropic dimensional changes. Because graphite is an optically uniaxial material, bireflectance can be used to determine the degree of preferred orientation of the graphitic crystallites. German and early U.S. TRISO fuel programs used an optical polarimeter to characterize the preferred orientation of the graphitic crystallites by measuring the relative reflected intensity of light polarized parallel and perpendicular to the preferred orientation, which typically aligned with the deposition direction. The ratio of maximum to minimum reflected intensity has been called the optical Bacon Anisotropy Factor (BAF_O) in deference to

the X-ray-derived Bacon Anisotropy Factor developed as a measure of the degree of orientation in graphite (Bacon 1956).

However, the optical polarimeter method was flawed and significant variations were observed in a round-robin test of seven polarimeters historically used for TRISO characterization in Germany, France, and the U.S. (Stevens 1979). Therefore, the AGR program has used diattenuation data obtained with a two-modulator generalized ellipsometry microscope (2-MGEM) specifically developed for TRISO particle QC (Jellison and Hunn 2006, 2008). The optical anisotropy factor (OPTAF) can be derived as Equation (1):

$$\mathrm{OPTAF} = \frac{R_o}{R_e} = \frac{1+N}{1-N}, \quad (1)$$

where

R_o = is the reflectance of light polarized perpendicular to the optic axis

R_e = is the reflectance of light polarized parallel to the optic axis

N = is the diattenuation, defined as

$$N = \frac{R_e - R_o}{R_o + R_e}$$

The polarimeter-derived BAF_O was intended to be equivalent to the physical OPTAF, but polarization perturbations present in the optical elements of the polarimeters used to measure BAF_O introduced error in the analyses. To relate the historical database to the results measured by the AGR program, a correlation between diattenuation and the historically measured BAF_O is needed. Two correlations have been used by the AGR program to cross-correlate diattenuation with the polarimeter-derived BAF_O. An early correlation was based on the mathematical form of the first-order Taylor series expansion for the OPTAF (i.e., OPTAF ≈ 1 + 2N for small N). A correlation factor for the diattenuation was determined by comparing reported data from measurements of the IPyC and OPyC BAF_O in all eight batches of the German proof test particle composite EUO 2358–2365 using the Hochtemperaturreaktor-Brennelement GmbH (HOBEG) optical polarimeter (Hantke 1992) to PyC optical anisotropy data obtained using the ORNL 2-MGEM for particles from an archive of the same proof test composite (Hunn 2004b). On average, the diattenuation values that would have yielded OPTAF values equivalent to the BAF_O values obtained from the HOBEG polarimeter were 1.4 times higher than the diattenuation values measured with the ORNL 2-MGEM for the IPyC and 1.6 times higher for the OPyC. Because the early AGR program specifications used values based on the HOBEG polarimeter-derived BAF_O, an equivalent BAF_O value (equiv_BAF_O) was defined to correlate the diattenuation measured with the 2-MGEM to the polarimeter-derived BAF_O values in the specification (see Equation [2]).

$$\text{Correlation 1: equiv\_}BAF_O \approx 1 + 2 \times (1.5 \times N) = 1 + 3N, \text{for small N} \quad (2)$$

The diattenuation correlation factor of 1.5 was based on the comparisons discussed above to estimate from the 2-MGEM-measured diattenuation what might have been measured, on average, if the HOBEG polarimeter was used to analyze the same sample (Hunn 2005).

A more accurate correlation was derived later as an outcome of a comparison of the ORNL 2-MGEM with the Commissariat à l'Énergie Atomique (CEA) optical polarimeter technique called RAPAX (Jellison et al. 2010). As part of this study, measurements were performed on two optical standards with known diattenuation: an aluminum mirror with N = 0 and an appropriately oriented single crystal of rutile with N = 0.085 ± 0.002 at 640 nm (the wavelength of light used for RAPAX) and N = 0.087 ± 0.002 at 577 nm (the 2-MGEM wavelength). No evidence has been found as to whether historical polarimeters included the use of optical standards to correct for polarization effects or to verify the accuracy of the measured optical anisotropy. Standard operation of the 2-MGEM ellipsometer includes a calibration step using an aluminum mirror to cancel out minor polarization perturbations from the optics and effects

related to the photoelastic modulator-polarizer pairs, which are the heart of the generalized ellipsometer. Validation of the 2-MGEM system using rutile is also common practice (Jellison, Hunn, and Lowden 2006).

Insertion of the aluminum mirror in the RAPAX sample position revealed that polarization effects in the polarimeter optics were introducing an error in the measured results. Mueller matrix calculations were performed to model the polarization introduced by certain optical components. The beam splitter had a particularly strong effect, but other optics, such as the microscope objectives, also affected the polarization state of the light directed to and reflected from the sample. These calculations led to the determination that, to first order, the incorporated error in the polarimeter-derived BAF_O took the mathematical form of a simple multiplicative factor (F), as shown in Equation (3).

$$\text{Correlation 2: Polarimeter\_BAF}_O \approx F \times OPTAF = F \times \frac{1+N}{1-N} \quad (3)$$

The value of F can be obtained directly from the measured Polarimeter_BAF_O of an aluminum mirror since N = 0 for the mirror. Measurements with the RAPAX of an aluminum mirror gave an error factor of F = 1.082 ± 0.001. Incorporating this error factor in the derivation of the rutile diattenuation from the RAPAX-measured BAF_O reduced the deviation from the known value at 640 nm from +38% to –8%. For comparison, the calibrated 2-MGEM measured an average diattenuation of N = 0.0885 ± 0.0017 for rutile, which is within the uncertainty of the known value for 577 nm.

The value of F is polarimeter-dependent. For the HOBEG polarimeter, the correction factor F was estimated to be F ≈ 1.010 ± 0.006 by comparing the reported IPyC and OPyC BAF_O in all eight batches of the German proof test particle composite EUO 2358–2365 (Hantke 1992) to measurements of two sets of ten particles each from an archive of the same proof test composite using the ORNL 2-MGEM. Results of an earlier round-robin comparison between the HOBEG and GA polarimeters also showed a discrepancy in the measured BAF_O (Saurwein 1995). The data reported by GA suggest a correction factor of F ≈ 1.025 for the GA polarimeter.

The specifications for AGR-1 and AGR-2 PyC anisotropy were based on historical TRISO fuel PyC layer performance versus polarimeter measurements of BAF_O. For AGR-1, both IPyC and OPyC were required to have a mean $BAF_O \leq 1.035$ at 95% confidence with ≤1% in a critical region of ≥1.06. The mean optical anisotropy allowance was increased for the AGR-2 IPyC layer to $BAF_O \leq 1.045$ to allow for more leeway in achieving an allowable IPyC anisotropy without driving the density too low. This change was supported by a review of historical data that indicated acceptable irradiation performance of TRISO particles with IPyC anisotropies above a BAF_O of 1.035. German particles had IPyC BAF_O as high as 1.053 and still displayed excellent irradiation performance (Petti et al. 2004). The higher anisotropy limit for IPyC compared with OPyC was also justified recognizing that SiC deposition increases the IPyC anisotropy. For acceptance testing of AGR-1 and AGR-2 TRISO particles, Correlation 1 (Equation 2) was used to calculate equiv_BAF_O from the measured diattenuation, and these values were compared to the specified limits.

For AGR-5/6/7, the fuel specification for PyC anisotropy evolved from the polarimeter-based BAF_O values to the fundamental property of diattenuation used in optical physics. The limits for PyC BAF_O in the AGR-2 fuel specification were converted to diattenuation limits using Correlation 2 (Equation 3) and the error factor of F = 1.010, which was estimated for the HOBEG polarimeter. Specifically, the mean and critical region limits for BAF_O of ≤1.035, ≤1.045, and ≥1.060 were converted to N of ≤0.0122, ≤0.0170, and ≥0.0242, respectively.

The optical anisotropy of the pyrocarbon layers has historically been measured on the TRISO particles before the particles are encapsulated and heat treated as fuel compacts or spheres. It is recognized that heat treating the compacts at 1800°C for one hour causes an upward shift in the optical anisotropy of both pyrocarbon layers. Data on this increase has been documented for AGR fuel particles

in support of future evolutions of the specification (Hunn, Jellison, and Lowden 2008; Hunn, Savage, and Silva 2010, 2012; Helmreich et al. 2017).

The variability of the historical polarimeter data, which is especially evident in the round-robin study (Stevens 1979), and the need for a polarimeter-dependent correction factor to account for perturbations in the optical elements (Jellison et al. 2010) emphasizes the tenuous nature of the specification basis using the historical polarimeter data and may explain comments regarding inconsistencies of performance versus BAF_O (Bullock and Young 1994). The historic polarimeter measurement uncertainties also challenge the connection of the data used to generate early pyrocarbon anisotropy specifications to the higher integrity ellipsometry measurements because the historic polarimeters are not available to determine the appropriate correction factor using calibration standards. Diattenuation using current ellipsometry methods is preferred going forward, but a specific database of fuel performance relative to current diattenuation measurements is limited to the AGR program, and possibly to German/USHTGR fuel that has been re-evaluated with the 2MGEM. Additional irradiation testing of samples measured with modern methods would be necessary to further refine the specified anisotropy criteria by removing uncertainties associated with the historic polarimeter measurements.

2.3.7 Defective IPyC Fraction

Defective IPyC is defined as layers that allow excessive permeation of chlorine compounds generated during SiC deposition through the IPyC, resulting in unallowable levels of uranium transport into the surrounding carbon layers. Uranium transport due to chlorine attacking the kernel is typically not manifested until the particle temperature is elevated sufficiently. The highest fabrication temperature occurs during the heat treatment of the fuel compacts (1800°C for AGR compacts); therefore, analysis for defective IPyC is performed after this thermal exposure. Particles are defined as having defective IPyC if the X-ray density in an X-ray radiograph from uranium outside the kernel exceeds a specified limit. U.S. fuel specifications have used visual standards to define the amount of uranium dispersion indicative of defective IPyC. Visual standards produced by GA (Scheffel and Saurwein 2002, Figure 3) were used for the AGR-1 and AGR-2 fuel specifications. These were replaced in the AGR-5/6/7 fuel specification with example images generated during characterization of AGR-5/6/7 development batch 93069A (Figure 3).

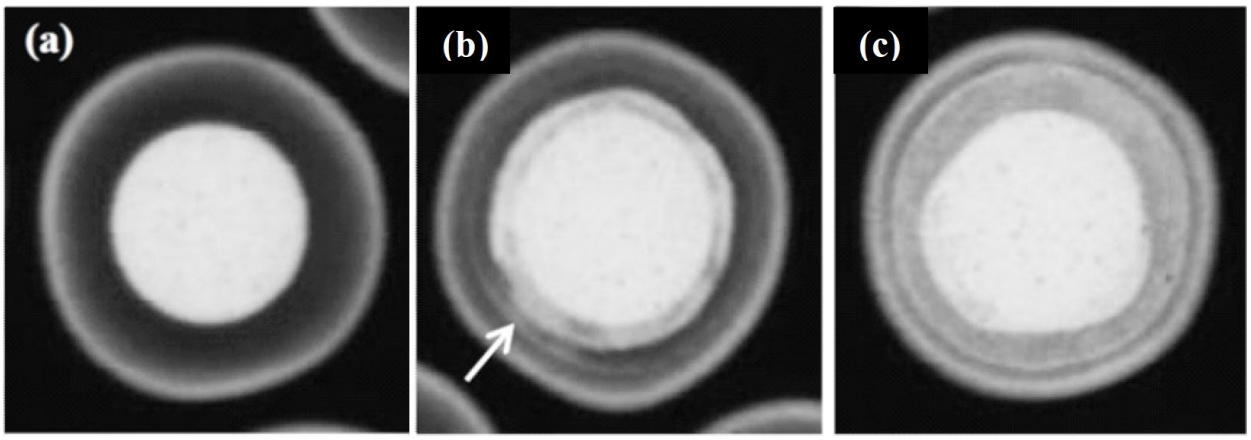

Figure 3. X-ray radiographs showing (a) a particle with acceptably low IPyC permeability and (b and c) particles with visible uranium dispersion from unacceptably high IPyC permeability (images from Marshall 2017).

Dispersion of uranium outside of the kernel may contribute to SiC layer defects during fabrication and threaten the integrity of the SiC layer by accelerating fission product attack during operation. The specification of $\leq 10^{-4}$ is intended to limit the number of particles susceptible to an increased probability of SiC failure due to fission product attack.

During the AGR-1 and AGR-2 fuel fabrication campaigns the defective IPyC fraction was determined using particles harvested from deconsolidated compacts after leach-burn-leach (described in Section 2.6.8). For AGR-5/6/7, the specification was applied instead to the TRISO-coated particle lots, using particles that had been heated to 1800°C for 1 hour to mimic the peak heat treatment step for compacts. The new approach allowed large populations of particles to be easily obtained for analysis with less effort than those obtained from deconsolidating compacts. This approach was justified by the fact that the compacting process does not impact the IPyC defect fraction other than by providing the heat needed to produce the visual evidence of particles that have experienced excessive chlorine intrusion.

2.4 Silicon Carbide Layer

2.4.1 SiC Purpose

The silicon carbide layer provides the structural, load-bearing support needed to ensure particle integrity during particle handling, compact formation, and irradiation. The silicon carbide is impermeable to most fission products and functions as the primary fission product retentive layer in the TRISO particle.

2.4.2 SiC Deposition

Silicon carbide in the AGR-5/6/7 TRISO particles was deposited by the hydrogen-assisted thermolysis of methyltrichlorosilane (CH_3SiCl_3, MTS) in a pulsatory spouted bed at bed temperatures near 1565°C. The MTS was vaporized in a stream of hydrogen and further diluted with argon. The argon to hydrogen ratio was 30:70 and the coating gas fraction in the inlet gas stream was approximately 0.03 (Marshall 2020). AGR-1 Variant 3 and AGR-2 SiC layers were also deposited with an argon diluent (Phillips, Barnes, and Hunn 2010). The argon diluent enables a somewhat lower deposition temperature without incurring superstoichiometric silicon in the deposit and a finer SiC grain structure than is usually obtained with MTS in pure hydrogen without also introducing excessive free silicon. The presence of argon also improves fluidization of the particle bed. The decomposition products are SiC and HCl via a chain of intermediate reactions. Deposition is thought to occur primarily as a surface reaction (heterogeneous nucleation) on the fuel particles. The density of the SiC layer is usually about 3.2 g/cm^3, and the layer deposition rate is typically near 0.37 μm/min.

2.4.3 SiC Specifications

SiC layer specification are given in Table 4.

2.4.4 SiC Thickness

A mean thickness for each SiC layer in a random sample of TRISO-coated particles is determined by cross sectioning the particles to near midplane and analyzing optical micrographs of the polished cross sections with automated image analysis. The SiC layer is the primary structural layer within the TRISO particle. The SiC layer provides most of the mechanical strength during fuel fabrication and the hoop strength during irradiation. In addition, this layer provides significant retention of fission products. The GA MHTGR fuel specification for SiC thickness requires a mean range of 30–40 μm, with a target of 35 μm, based on (1) the need to accommodate anticipated stresses in the layer during irradiation, (2) the provision for adequate thickness to restrict fission product release, and (3) the need for adequate particle strength to limit particle defects created during compact fabrication (Scheffel and Tang 1989). Thermomechanical modeling of particle behavior early in the development of the AGR-1 fuel specification indicated that a lower critical limit of 20 μm was sufficient to restrict particle failure to acceptable levels, but this limit was increased to 25 μm to provide a margin for SiC degradation (or "thinning") due to reactions with fission products (Petti et al. 2004). The specification was also tightened

to require a mean of 32–38 μm to ensure the normal distribution in the SiC thickness for coating batches with a mean thickness near the lower limit on the mean does not significantly extend below the lower critical limit for the population. The AGR-5/6/7 fuel specification subsequently utilized a modified and slightly more conservative lower critical limit of 28 μm to limit very low thicknesses based on observations of particle damage during handling (TCT 2012).

Table 4. Silicon carbide layer specifications for the TRISO particle lot.

Property	Specification	Possible Consequence
Thickness (μm)	$32 \leq \bar{x} \leq 38$ $\leq 1\% \leq 28$	**Below LL_P**—Inadequate strength to withstand internal pressure and compaction forces.
Sink-float density (g/cm^3)	$3.19 \leq \bar{x}$ $\leq 1\% \leq 3.17$	**Below LL_P**—Impaired retention of fission products and reduced strength.
Aspect ratio[a]	$\leq 1\% \geq 1.14$	**Above UL_P**—Non-uniform stresses and high stress concentrations in SiC layer.
Microstructure	Grain size < visual standard	**Above Limit**—SiC with diminished fission product retention and/or poor physical properties.
SiC inclusions[b]	Information only	**Above Limit**—Oddly shaped layer or abnormal SiC microstructure may be more susceptible to failure.

a. Aspect ratio is measured after removal (burn back) of the OPyC layer by heating in air at 750°C–850°C.

b. A maximum allowed defective fraction of particles with SiC inclusions (a.k.a. gold spots) was included in the AGR-1 and previous GA TRISO particle specifications (see Section 2.4.8 for further discussion).

2.4.5 SiC Density

The sink-float density of each SiC fragment in a random sample of fragments taken from a TRISO particle lot is determined by measuring the neutral buoyancy position in a linear-gradient density column. The strength and impermeability of the SiC layer is associated with the density of the SiC. The incorporation of superstoichiometric Si or C into the SiC lattice structure decreases the SiC density and may enhance the transport of some elements through the SiC layer. The incorporation of voids within the layer also decreases the average density and provides regions of potentially rapid fission product transport. The theoretical room temperature density of 3C-SiC (β-SiC) is 3.215 g/cm^3 (Snead et al. 2007). In the GA GT-MHR fuel specification, a lower limit on the mean equivalent to ~99% of the theoretical density (3.18 g/cm^3) was specified to restrict the allowable deviation from good stoichiometry and low porosity needed for adequate structural strength and retention of fission products. A lower critical limit of no more than 1% of the population with densities below 3.17 g/cm^3 was specified to minimize the fraction of the population with low density while remaining within the capability of the GA process to meet the specification. Results from studies of the SiC mechanical, microstructural, and thermochemical properties and irradiation performance were used to support these limit selections (Bullock and Young 1994).

The SiC coating process used for the AGR program supported the increase of the lower limit on the mean to 99.2% of the theoretical density (3.19 g/cm^3). For example, the measured sample from the AGR-5/6/7 coated particle composite had a mean SiC density of 3.195 g/cm^3 and a standard deviation of 0.002 g/cm^3. This yielded a 95% confidence interval on the mean with lower and upper values of 3.1945 and 3.1949, respectively, which satisfied the $3.19 \leq \bar{x}$ lower limit on the mean and a 1% tolerance lower critical limit as high as 3.1913 g/cm^3 (Marshall 2020).

2.4.6 SiC Aspect Ratio

The SiC aspect ratio is characterized in the same manner as the kernel aspect ratio (Section 2.1.6). Coated particles that deviate from spherical geometry will experience localized increase in the stress in

the SiC layer that can impact particle failure probability (Miller and Wadsworth 1994; Miller, Petti, and Maki 2004). To minimize the impact of this effect, specifications are placed on the particle aspect ratio, which is defined as the ratio between the maximum and minimum diameter in a projected image of a particle. The requirement that ≤1% of particles exceed an aspect ratio of ≥1.14 was established during the evolution of the AGR-1 fuel specification and was based on computational modeling of fuel performance that related the particle aspect ratio to the predicted particle failure probability (Barnes 2006). This value was retained for both AGR-2 and AGR-5/6/7 fuel specifications, although the specification was revised so that it was applied to the SiC layer and not the OPyC layer as in the AGR-1 specification. During development of the AGR-5/6/7 fuel specification, AGR program staff noted that BWXT was fabricating fuel with 1% of the particles exceeding an aspect ratio of approximately 1.08, which was significantly below the UL_P specification of 1.14 (Marshall 2012). This resulted in the suggestion that the specification could be tightened to a UL_P of ≤1% ≥1.10; however, such a change was not implemented. The AGR-5/6/7 fuel ultimately had 1% of the particles with an aspect ratio ≥1.0735 (Pham et al. 2021).

2.4.7 SiC Microstructure

Early experience in the fabrication of CVD SiC for coated particles was summarized by Price (1977). The review by Price included an examination of the impact of SiC deposition temperature on layer microstructure, properties, and irradiation performance. While it was noted that several deposition process variables are involved in determining SiC microstructure, a key finding was that SiC deposited below ~1500°C may contain multiple SiC polytypes (besides pure β-SiC), free Si, and a laminar structure with high porosity that results in high fission product diffusivity. On the other hand, unacceptably low layer densities could result when deposition temperatures exceed 1700°C. Thus, it was recommended that deposition temperatures ≥1500°C but ≤1700°C be used to achieve high-density SiC (i.e., >99% of theoretical density). However, it should be noted that this temperature range was established for a process using pure hydrogen and MTS for SiC deposition. Temperatures below 1500°C produce acceptable microstructure when the deposition process includes an argon diluent. The AGR-1 Variant 3 SiC was deposited at 1425°C with a 1:1 H_2-to-Ar gas ratio (Hunn and Lowden 2006).

At the inception of the AGR program, the nature of the TRISO SiC-layer microstructure was evaluated to establish the requirements for AGR fuel specifications (Petti et al. 2002). The SiC microstructure of previous U.S. fuel fabrication efforts was compared with historic German fuel that was considered the best point of reference at the time for high-quality TRISO fuel with good in-pile performance. The German SiC was deposited at a lower temperature (1500°C vs. 1650°C) than was used in the U.S. to fabricate the New Production-Modular High Temperature Gas-Cooled Reactor (NP-MHTGR) performance test fuel irradiated in some of the High Flux Isotope Reactor Removable Beryllium (HRB) and ATR irradiations that showed relatively higher in-pile failure fractions.[†] It was recognized that the 1500°C deposition temperature resulted in a slower layer growth rate and smaller, equiaxed grains compared with the columnar grains produced at 1650°C. Petti et al. (2002) cited earlier U.S. fuel fabrication and irradiation efforts (Bullock 1984) examining the performance of different kernel compositions and SiC microstructures. The effect of SiC grain size on fission product release was complicated by the use of different SiC microstructures with different kernel compositions; however, the author concluded that "there was evidence that Ag release was enhanced in coatings having large-grained columnar structure" (Bullock 1984). Thus, a high-density SiC layer with relatively equiaxed grains was considered desirable. Several U.S. reports generated in the mid-1990s identified the need to reduce the SiC deposition temperature to around 1500°C and to avoid large columnar grain structure (Bullock and Young 1994; Munoz 1994), which was consistent with an earlier report (Federer 1977). However, work in the U.S. was halted in the mid-1990s before these changes could be applied. After review of the data, the study by Petti et al. (2002) ultimately determined that "while clearly not conclusive, grain structure

[†] The failures in the NPR and HRB-21 irradiations were determined to be related to the pyrocarbon layers and interactions with the matrix, and not from deficiencies in the SiC layer (Maki et al. 2002).

appears to be important to fission product retention." The conventional understanding at the time was that large, columnar grains are not preferrable because the associated grain boundaries, oriented in a radial direction across the SiC layer, present a lower barrier to fission product diffusion through the layer compared to microstructures with smaller, equiaxed grains that result in tortuous grain boundary pathways.

While the importance of the SiC layer grain size was recognized, SiC microstructure properties were not included in TRISO fuel specifications prior to 2000. In the early 2000s, the AGR program pursued a SiC grain size smaller than the previous U.S. efforts and closer to the German SiC microstructure. A qualitative specification was established to verify that large, columnar SiC grains like those present in the NPR performance test fuel were not present in a sufficiently representative sample of AGR irradiation test fuel by comparing backscattered electron images of the SiC grain structure to a visual standard that represented an unacceptably large average grain size, particularly in the radial direction (Figure 4, Barnes 2006). A SiC deposition temperature of 1500°C was used for the AGR-1 baseline SiC, the same as the German process, both of which also used pure hydrogen and MTS for the deposition. A visual standard for unacceptably large SiC grains was obtained from SiC deposited with the ORNL 50-mm-diameter fluidized-bed CVD coating system at 1560°C using MTS and pure hydrogen. The large, columnar grains evident in this visual standard were similar to those observed in an archive sample of the fissile TRISO particle fuel (8876-70) fabricated at GA and irradiated in the HRB-21 experiment (Goodin, Kania, and Patton 1989; Scheffel et al. 1991). Visual standards for the target equiaxed SiC grain structure and an undesirably small average grain size were produced (Hunn 2013; Barnes 2006, Rev. 2). These standards were eventually dropped from the final AGR-1 fuel specification (Barnes 2006, Rev. 8) because their intent was only to limit the acceptance of TRISO particle lots exhibiting unacceptably large, columnar grains expected to adversely impact fission product retention. No lower limit specification on SiC grain size was deemed necessary since this was effectively controlled by the density specification. SiC layers with very small grains tend to have excessive porosity that will cause the density to be below specification.

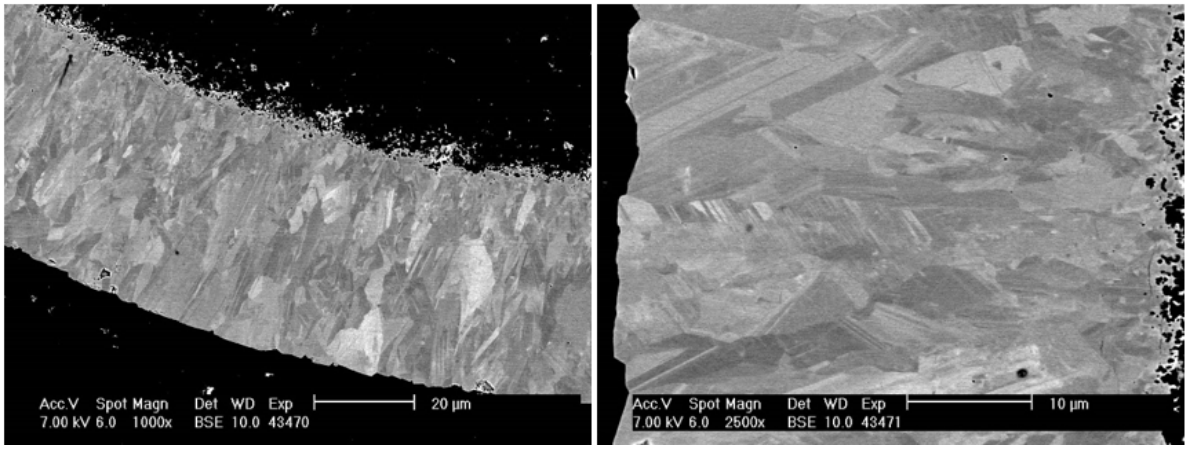

Figure 4. Examples of unacceptable SiC with excessively large columnar grains spanning half the layer thickness (images from Barnes 2006).

Fuel characterization efforts undertaken following fabrication of the AGR-5/6/7 fuel have included the development of a QC method capable of rapid quantitative analysis of SiC grain structure using image analysis (Helmreich et al. 2020b). This approach offers an opportunity to evolve from a subjective, qualitative comparison against visual standards to an objective, quantitative method for specification and acceptance testing of SiC grain size.

As discussed above, smaller, equiaxed grains are considered preferable to large, columnar grains based on fission product retention behavior. However, microstructures with extremely fine SiC grains

resulting in a relatively high density of grain boundaries may offset the benefit of the tortuous transport pathways to restrict fission product migration. Data from the AGR-1 and AGR-2 experiments indicate that silver diffused more readily through the finer grained SiC deposited with an argon diluent in the AGR-1 Variant 3 and AGR-2 particles than it diffused through the more medium-sized grains of the SiC deposited at 1500°C in the AGR-1 Baseline, Variant 1, and Variant 2 irradiation test fuel using MTS in pure hydrogen (Lowden 2006; Hunn, Savage, and Silva 2012). This difference was presumably due to the greater density of grain boundaries in the finer grained SiC. However, this effect was only readily observed when the irradiated compacts were heated to 1800°C for more than 100 hours (Morris et al. 2014). There was no observable difference in fission product transport between these two microstructures under any other conditions, including irradiation or 300-hour post-irradiation heating tests at 1600°C and 1700°C.

2.4.8 SiC Inclusions

A maximum allowed defective fraction of particles with SiC inclusions (called "gold spots") was included in the AGR-1 and previous GA TRISO particle specifications (Barnes 2006; Munoz 1994). After removing the OPyC layer by heating TRISO particles in air at temperatures of 750°C–850°C, light penetrating through large-grained SiC reflects off low-density inclusions in the layer and creates the appearance of white or gold spots on the exposed SiC surface (Figure 5). These inclusions can be formed by fluidization anomalies during coating if particles become trapped in stagnant regions in the fluidized bed or if they pick up carbon soot from the coating chamber walls. Inclusions of carbon soot, carbon soot infiltrated with SiC, and low-density SiC have been observed. These inclusions are typically localized to one area, and thicker inclusions result in asymmetric coated particle shapes. At the extreme limit, carbon soot inclusions infiltrated with SiC can produce thick regions of low-density SiC that present a weakened barrier to fission product release. Elevated fission product release has been observed from particles with soot inclusions that led to SiC fracture during AGR-1 safety tests (Hunn et al. 2014).

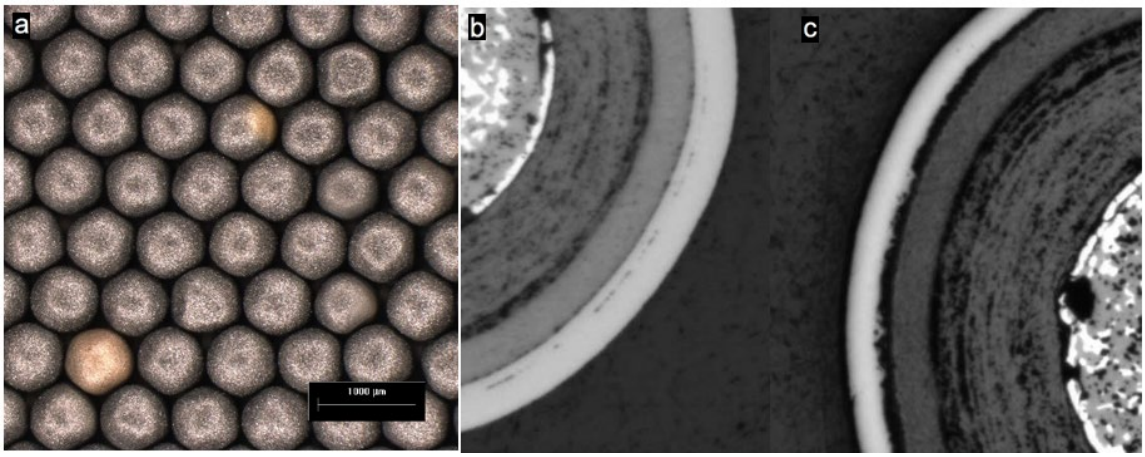

Figure 5. Optical micrographs showing (a) particles with gold spots visible when light is reflected from the exposed SiC layer after removal of the OPyC (image from Barnes 2006), (b) a cross-sectioned particle with a soot inclusion in the SiC, and (c) a cross-sectioned particle with a soot inclusion at the IPyC-SiC interface (images from Hunn 2008).

The finer-grained SiC microstructure deposited in AGR-1 Variant 3, AGR-2, and AGR-5/6/7 TRISO particles scatters more of the transmitted light such that soot inclusions do not manifest as visible gold spots. Therefore, an alternate QC method was developed to observe and enumerate soot inclusions in thousands of cross-sectioned particles (Hunn 2008).

For AGR-2 and subsequent fuel specifications, the fraction of particles with soot inclusions was included as a required measurement for information only. Reasons for deleting the acceptance criteria for soot inclusions are discussed in the AGR-2 fuel specification (Barnes 2009) and include good in-pile performance of AGR-1 test fuel with gold spot populations near the specified limit, low levels of soot inclusions in three AGR-2 development batches, and uncertainties in defining the acceptance limit. Information on the population of particles with soot inclusions was collected for AGR-1 (Hunn, Savage, and Silva 2012), AGR-2 (Barnes and Marshall 2009), and AGR-5/6/7 (Helmreich et al. 2017) irradiation test fuels to support the possibility of future reinstatement of this specification based on input from the irradiation testing and PIE of the irradiated particles.

2.5 Outer Pyrocarbon Layer

2.5.1 OPyC Purpose

The purpose of the OPyC layer is to protect the SiC layer from mechanical damage after coating (during handling, overcoating, and compacting) and to provide an additional barrier against fission product release, particularly in a particle with a through-layer SiC defect or failure in which an intact OPyC layer may be the last hermetic seal preventing excessive gas release and reduction of the kernel's chemical stability. In the AGR-1 and AGR-2 experiments, the OPyC usually remained intact and continued to provide excellent retention of fission gases in the rare instances of SiC layer failure (Demkowicz et al. 2015; Stempien et al. 2021). It has conventionally been understood that the OPyC layer contributed to the compressive stress in the SiC layers as the OPyC shrinks during irradiation. However, data from the AGR-1 and AGR-2 experiments suggest that, in some cases, the OPyC may separate from the SiC layer as it densifies during irradiation and the inner radius increases. This separation is a consequence of a weak SiC-OPyC interface bond in combination with a strong OPyC-matrix bond (Hunn et al. 2013, 2015; Stempien et al. 2021). In such a scenario, the OPyC layer would not contribute a compressive load on the SiC layer. Nonetheless, this does not significantly affect the overall stress in the SiC layer; more recent computational modeling indicates that most of the compression of the SiC layer comes from IPyC shrinkage and not OPyC shrinkage. The OPyC layer also prevents bonding of the graphitic fuel element matrix with the SiC layer or the direct transmission of mechanical stresses from matrix growth or shrinkage during thermal- or irradiation-induced dimensional changes.

2.5.2 OPyC Deposition

The OPyC layer is intended to have the same physical properties as the IPyC layer. The OPyC was deposited with the same propylene-to-acetylene ratio but with a 5% higher total coating gas concentration, resulting in an argon diluent fraction of 0.685 (Marshall 2020). Changes in particle properties (e.g., thermal conductivity, density, and diameter) through the course of the deposition and particle circulation rates within the bed necessitated a higher deposition temperature (~1350°C) than was used for the IPyC layer. A greater bed surface area is associated with the larger particle diameter and resulted in a lower pyrocarbon deposition rate (2.4 μm/min).

2.5.3 OPyC Specifications

OPyC layer specifications are shown in Table 5.

Table 5. Outer pyrocarbon layer specifications for the TRISO particle lot.

Property	Specification	Possible Consequence
Thickness (μm)	$36 \leq \bar{x} \leq 44$ $\leq 1\% \leq 20$	**Below LL_P**—Reduced mechanical protection of the SiC layer during handling. Reduced fission product retention in particles with failed SiC.
Sink-float density [a] (g/cm^3)	$1.85 \leq \bar{x} \leq 1.95$ $\leq 1\% \leq 1.80$ $\leq 1\% \geq 2.00$	**Below LL_P**—Permeable layer, which could result in higher fission product release from particles with failed SiC. Greater bond strength with matrix. **Above UL_P**—Associated with increased anisotropy.
Diattenuation	$\bar{x} \leq 0.0122$ $\leq 1\% \geq 0.0242$	**Above UL_P**—Uneven shrinkage; induced stress in OPyC layer.
Defective OPyC fraction	$\leq 3.0 \times 10^{-4}$	**Above Limit**—Mechanical damage to SiC during handling and direct contact with matrix.
a. Density specifications are specific to density measured by sink-float technique.		

2.5.4 OPyC Thickness

A mean thickness for each OPyC layer in a random sample of TRISO-coated particles is determined by cross sectioning the particles to near midplane and analyzing optical micrographs of the polished cross sections with automated image analysis. The OPyC layer provides a mechanically protective layer over the SiC to reduce the likelihood of the SiC layer cracking or breaking during TRISO particle handling and compaction. It isolates the SiC layer from direct contact with the matrix and greatly reduces stresses to the SiC layer from anisotropic dimensional changes in the matrix. The OPyC layer also functions as a barrier to fission product migration and release from the TRISO particle. A properly deposited SiC layer has low surface porosity and relatively low surface roughness, so the OPyC layer forms a weak bond with the SiC substrate.

While the purpose of the OPyC layer is not identical to that of the IPyC layer, the rationale for establishing the specifications is similar. The specification for the mean is intended to provide a layer with adequate durability to protect the SiC layer, retain fission gas in the event of a SiC layer failure, and contribute to compressive stress in the SiC layer during irradiation, while avoiding excessive thickness that could result in high irradiation-induced stresses in the OPyC layer and increase the probability of layer failure (Scheffel and Tang 1989; Petti et al. 2004). The LL_P specification (≤1% ≤20 μm) is established to limit the population of particles with an extremely thin OPyC layer that could exhibit high permeability to fission gases.

2.5.5 OPyC Density

Sink-float density of each OPyC fragment in a random sample of fragments taken from a TRISO particle lot is determined by measuring the neutral buoyancy position in a linear-gradient density column. The basic technical considerations regarding OPyC density and its relationship to structural anisotropy are the same as those already discussed for the IPyC layer (Section 2.3.5). A sufficiently high pyrocarbon density is beneficial to limit the layer permeability to fission gases in the event of a particle having a defective or failed SiC layer. U.S. fuel specifications predating the AGR program also considered the surface porosity and layer strength (both of which can be related to density) as a concern with respect to bonding with the matrix, which could result in OPyC fracture and impact particle performance (Scheffel

and Tang 1989). Such considerations dominated the technical discussions on OPyC properties during the MHTGR program because of the nature of the compact formation process, which involved mixing coated particles with a viscous petroleum pitch binder which could significantly infiltrate OPyC layer open porosity (see additional discussion in Section 2.6.6).

The MHTGR fuel specification established that mean OPyC envelope densities between 1.80 and 1.95 g/cm^3 had adequate performance based on previous irradiation testing (Scheffel and Tang 1989). The GT-MHR fuel specification included a mean OPyC envelope density requirement of 1.75–1.90 g/cm^3 and noted the range for OPyC sink-float density was yet to be determined (Munoz 1994). The GA preliminary AGR fuel specification provided recommendations for both envelope density of 1.76–1.90 g/cm^3 and sink-float density of 1.85–1.95 g/cm^3 (Scheffel and Saurwein 2002). This sink-float density range was adopted for all AGR program specifications. The lower critical limit for the OPyC sink-float density used by the AGR program (≤1% ≤1.80 g/cm^3) was also adopted from the GA preliminary AGR fuel specification.

Fuel performance modeling using PARFUME indicates that the probability of SiC failure exhibits negligible dependence on OPyC density (Petti et al. 2004; Skerjanc 2016). As a result, there is not a strong technical basis for an upper critical limit on the OPyC layer density. The AGR program, therefore, adopted the same upper critical limit that was established for the IPyC layer using particle performance modeling based on the need to achieve satisfactory creep behavior.

Post-irradiation observations of AGR-1 and AGR-2 coated particles have challenged some of the previous understanding of coating layer behavior. The matrix formulation and compact forming methods used to fabricate the AGR fuel are substantially different than previous U.S. experience, such that pitch binder infiltration into the OPyC layer is no longer a concern. However, observations of irradiated and safety tested particles indicate that the OPyC-matrix bond may be sufficiently strong—and the SiC-OPyC bond may be sufficiently weak—that the layer remains bonded to the matrix and can separate from the SiC layer during radiation-induced shrinkage of the OPyC and matrix (Stempien et al. 2021). In such a case, the OPyC would no longer contribute to compressive stress in the SiC layer. However, in spite of the bond between the OPyC and the matrix in the AGR particles, OPyC failure has not been observed. This is likely influenced by the overall level of OPyC layer shrinkage in the AGR fuel, which is dependent on density and structural anisotropy.

2.5.6 OPyC Anisotropy

The basis for the OPyC diattenuation specification is discussed in Section 2.3.6.

2.5.7 Defective OPyC Fraction

The defective OPyC coating fraction is determined by a visual examination of a population of TRISO particles to detect broken or missing OPyC layers. The OPyC layer is the final defense against fission product release from the TRISO particles with defective SiC. A broken or missing OPyC layer also serves as an indirect indicator for potential damage to the SiC layer. An upper limit on the defective OPyC fraction is specified for the TRISO particle lot and the compact lot. The defective OPyC fraction specification was set at ≤0.01 for the fuel compacts (see Section 2.6.8) but at ≤3.0×10^{-4} for the TRISO particle lot used for compact fabrication. The higher limit for broken or missing OPyC layers after deconsolidation from the compacts allows for some OPyC layer damage during compact fabrication (i.e. in the processes of overcoating the TRISO particles with resinated-graphite powder and forming the compacts) or during compact deconsolidation.

The lower limit specified for the TRISO particle lot is to (a) control the quality of the coating process, (b) limit direct contact with the SiC layer that could cause SiC damage during TRISO particle handling, overcoating, and compacting, and (c) minimize the probability of a particle with a defective SiC layer also having a missing OPyC layer. The value is consistent with previous MHTGR (Tang 1989) and GT-MHR

(Munoz 1994) fuel specifications and falls between the previously used values of 1×10^{-4} (for core segment mean) and 1×10^{-3} (for compact lot mean). The probability of pressure vessel failure as a result of a missing OPyC for particles with normal SiC is very low, so the allowed $\leq 3.0 \times 10^{-4}$ fraction of particles with missing or defective OPyC does not contribute significantly to overall pressure vessel failure (Scheffel and Tang 1989). Quantification of OPyC defects after compacting determines if damage is caused by an aberrant post-coating process that is overstressing the TRISO particles. The higher defect fraction is justified in that particles in the compact with broken OPyC but no indication of SiC damage do not significantly affect irradiation performance. After compaction, the OPyC layer has already performed its primary role to protect the SiC; subsequently, the matrix provides protection against mechanical damage to the SiC.

2.6 Fuel Compact

2.6.1 Compact Purpose

TRISO-coated particles are typically embedded into a final fuel form whose size and shape can vary depending on reactor design. As previously discussed, the AGR program tested compacts formed into right cylinders with a matrix of graphite flake and carbonized resin filling the interstitial space between the TRISO particles. The graphite and carbonized resin matrix serves to protect the particles and retain them in a consistent geometry during operation and provide a pathway for heat removal from the particles. The matrix also serves as one of the key barriers to fission product release from the core. While certain elements (e.g., fission gases and volatile elements such as iodine) exhibit very little retention in the matrix, other elements (e.g., strontium and europium) can be significantly retained (Demkowicz et al. 2015; Stempien et al. 2021). Consequently, this layer can significantly attenuate the total release of these fission products.

2.6.2 Compact Fabrication

TRISO-coated particles are formed into a solid body using a mixture of graphite flake and phenolic resin to form a continuous matrix. The particles are first overcoated with the matrix/resin precursor powder and then compacted into a right-cylindrical geometry under controlled temperature and pressure conditions. Heat treatment of the compact serves to drive off adsorbed moisture, carbonize the organic resin, and densify the compact to a stable geometry (Marshall 2020). The heat treatment schedule can be complex depending on the resin and forming process and culminates in a hold at the peak temperature of 1800°C for one hour. Cylindrical compacts, as utilized in the AGR program, are compacted and heat treated to their net shape, with no need for subsequent machining to achieve final dimensions.

2.6.3 Compact Specifications

An overview of the AGR compact specification is given in Table 6.

2.6.4 Compact Uranium Loading

Uranium in each sampled compact is measured by burning off the matrix and OPyC, mechanically pulverizing the SiC layers, burning off the exposed inner carbon layers, dissolving the oxidized kernels in acid, and measuring uranium content with Davies-Gray titration and mass spectrometry. The specified uranium loading will be dependent on the reactor and fuel form design. The required uranium loading per capsule for the AGR-5/6/7 experiment was 1.36 ± 0.10 gU for the end capsules (Capsules 1 and 5) and 0.90 ± 0.08 gU for the central capsules. This was done to facilitate capsule temperature control in all capsules and to ensure an adequate number of TRISO particles were present in the various targeted temperature ranges for acceptable statistics on fuel performance (Collin 2018b). These uranium loadings

approximated particle volumetric packing fractions of 40% and 25%, respectively. These packing fractions were determined from the uranium loading and were unspecified.

Table 6. Fuel compact lot specifications.

Property	Specification	Possible Consequence
Uranium loading ~40% PF (gU/compact)	$1.26 \leq \bar{x} \leq 1.46$	**Below LL_M**—Low heat generation rate. Uneven temperature distribution in the fuel block.
Uranium loading ~25% PF (gU/compact)	$0.82 \leq \bar{x} \leq 0.98$	**Above UL_M**—High heat generation rate and higher than expected fuel temperature. Uneven temperature distribution in the fuel block.
Diameter [a] (mm)	$0\% \leq 12.20$ $0\% \geq 12.44$	**Below LL_M**—Higher packing fraction and matrix density that could increase probability for particle damage.
Length [a] (mm)	$0\% \leq 24.40$ $0\% \geq 25.30$	**Below LL_M**—Higher packing fraction and matrix density that could increase probability for particle damage.
Matrix density (g/cm^3)	$1.65 \leq \bar{x}$	**Below LL_M**—Poor thermal conductivity. Greater irradiation-induced shrinkage.
Fe outside SiC (µg per compact)	$\bar{x} \leq 25$ $\leq 1\% \geq 100$	**Above UL_P**—Degradation of SiC layer at operating and accident temperatures.
Cr, Mn, Co, Ni outside SiC (µg per compact)	$\bar{x} \leq 50$ each $\leq 1\% \geq 200$ total	**Above UL_P**—Degradation of SiC layer at operating and accident temperatures.
Ca outside SiC (µg per compact)	$\bar{x} \leq 50$	**Above UL_M**—Negative impact on reactor/experiment neutronics.
Al outside SiC (µg per compact)	$\bar{x} \leq 50$	**Above UL_M**—Negative impact on reactor/experiment neutronics.
Ti + V outside SiC (µg per compact)	$\bar{x} \leq 240$ total	**Above UL_M**—Potential to catalyze carbonaceous materials and degrade SiC during operation.
Dispersed uranium fraction ($g\ U_{leached}$ / $g\ U_{sample}$)	$\bar{x} \leq 1.0 \times 10^{-5}$	**Above UL_M**—High fission product release during operation and accidents.
Exposed kernel fraction (kernel equiv. / particle count)	$\leq 5.0 \times 10^{-5}$	**Above Limit**—High fission product release during operation and accidents.
Defective SiC fraction (kernel equiv. / particle count)	$\leq 1.0 \times 10^{-4}$	**Above Limit**—High fission product release during operation and accidents.
Defective OPyC fraction (defects / particle count)	$\leq 1.0 \times 10^{-2}$	**Above Limit**—Increased likelihood of combining with SiC defect to make exposed kernel defect.
a. Specification of 0% above or below the given limit requires 100% inspection.		

2.6.5 Compact Dimensions

Fuel compact dimensions are dependent on the intended application. Historically, 50-mm-long compacts were used in Fort St. Vrain and other GA HTGR designs. The AGR program selected a 25-mm-long compact (with ~12.3 mm diameter) because uniformity in local particle packing fractions is more easily achieved with the shorter compacts, and cylindricity is generally not an issue. Longer compacts may display more variability in packing fraction along the axis due to nonuniformity in

compacting pressures unless a dual-action press is used. As the binder resins are softened and cured at elevated temperature during the thermal treatment of the compacts, stress relaxation and strain relief may occur as well as gravimetric creep until the resin is fully cured and rigid. For these reasons, the cylindricity of longer compacts should be verified. In addition, anecdotal evidence from Japan suggests that a 2:1 L/D ratio is optimal for automated compact handling in a production facility.

Tolerances on the compact dimensions are at the discretion of fuel block designers. In general, the cylinder diameter must be specified in conjunction with the fuel hole in the graphite block to ensure the gap around the compact is in a sufficient range for heat transfer without significant binding during fuel insertion and any planned removal of irradiated compacts from the block (Scheffel and Tang 1989). In addition to measurement of average diameter, a pass-through gauge may be needed to ensure the maximum effective diameter (accounting for any deviation from a right-cylinder shape) does not exceed the hole size.

For AGR-5/6/7 fuel compacts, the dimensional specifications were given on critical limits only, which were 12.20–12.44 mm in diameter and 24.40–25.30 mm in length, to ensure that the gas gap between the compact and the compact holder channel could be maintained, and that the overall length of the compact stack was not taller than the compact holder. These critical limits were specified at 0% tolerance, which requires 100% inspection of the compacts. To further improve uniformity of gas gaps within the different irradiation capsules, compacts were selected for the irradiation capsule based on their measured mean diameter, with compacts in a single stack exhibiting limited diameter variability. This provided consistent thermal gaps in each fuel stack to facilitate irradiation capsule fabrication and maximize the accuracy of the thermal model used to calculate in-pile fuel temperatures.

2.6.6 Compact Matrix Density

Average matrix density is determined by measuring a compact's radius and length to calculate the volume of the cylinder, measuring the compact mass, and deriving the total matrix volume and mass by subtracting the contribution from the particles in the compact. U.S. TRISO fuel specifications for matrix properties prior to 2000 were influenced by the method of matrix formation. This process involved filling a cylindrical mold with a mixture of fuel particles and graphite “shim” particles, and then injecting a viscous mixture of binder, additive, and graphite powder. Petroleum- or coal tar-derived pitch was used as the binder phase, and heat treatment of the green compacts drove off volatile species and carbonized the binder (Bresnik 1991). These fuel specifications either did not include matrix density explicitly or only included preliminary values (Munoz 1994). However, porosity in the matrix—as determined by metallographic inspection—was considered an important property that could impact compact structural integrity, irradiation stability, and thermal conductivity (Scheffel and Tang 1989). Based on unirradiated compact properties and data on irradiation performance, an MHTGR specification was established so that no more than 5% of the compacts in a lot had matrix void volume ≥45% (Scheffel and Tang 1989).

The matrix fabrication approach changed significantly at the start of the AGR program, shifting to a particle overcoating method similar to that used in Germany for fabricating spherical fuel elements and using a matrix precursor powder consisting of graphite flake and binder resin (Heit et al. 1985; Hantke 1992). However, while the particle packing fraction in the 50-mm-diameter fueled portion of German spherical fuel elements would typically range from approximately 6 to 10 vol%, a significantly higher packing fraction was needed for cylindrical fuel elements that would be used in a prismatic HTGR. The fabrication process involves pressing the overcoated particles to achieve a robust green compact, and avoiding damage to coated particles during this pressing step was a paramount consideration at this early stage in the program. As a result, relatively low compacting pressures were favored over considerations of achieving higher matrix densities during fuel development efforts early in the AGR program. Therefore, given the lack of U.S. specifications on matrix density in the past and the challenges associated with applying the overcoating compact fabrication approach with high particle packing fractions, the program did not adopt a matrix density specification for the AGR-1 experiment. Ultimately, the AGR-1 fuel

fabrication campaign resulted in average matrix densities of 1.22–1.34 g/cm^3 for the four compact lots irradiated in the AGR-1 experiment (Hunn, Savage, and Silva 2012) and the fuel performance was excellent (Demkowicz et al. 2018).

Having demonstrated the compact fabrication capabilities during the manufacture of the AGR-1 fuel, a matrix density specification of ≥1.45 g/cm^3 was established for the AGR-2 fuel. This was based on the goal of achieving a higher compact thermal conductivity (increasing heat transport from the fuel) and minimizing compact irradiation shrinkage (which would limit the change in the temperature control gaps between the compacts and the surrounding graphite and improve the ability to accurately calculate compact temperature during irradiation in ATR). This value was still below historic German pebble matrix densities (~1.75 g/cm^3) but represented a compromise between achieving higher matrix density and limiting particle damage during compact formation. The AGR-2 fuel compacts substantially exceeded the density specification, with average matrix densities of 1.56 and 1.68 g/cm^3 for the UCO and UO_2 fuel compacts, respectively (Hunn, Savage, and Silva 2010; Collin 2018a).

Entering the AGR-5/6/7 fuel fabrication effort, the compact fabrication process was modified as part of the overall AGR program fuel fabrication scale-up effort (Phillips et al. 2012). The matrix density specification was increased again to ≥1.65 g/cm^3 based, in part, on the German matrix density specification (mean value of 1.75 g/cm^3) and in the interest of further increasing compact thermal conductivity and minimizing irradiation shrinkage. The fuel compacts irradiated in the AGR-5/6/7 experiments had a matrix density of approximately 1.76 g/cm^3 (Pham et al. 2021).

2.6.7 Compact Impurities

The mass of each specified impurity is measured in randomly selected compacts by measuring the impurities dissolved in the acid leachates generated during the leach-burn-leach analysis described in Section 2.6.8. Compact impurity specifications help to protect the PyC and SiC layers from external degradation by chemical contaminants that may be present in the graphite and resin used to form the matrix or by contaminants incorporated in the compacts during fabrication and handling. While the impurities are specified and measured in the final heat-treated compacts, good practice includes procurement specifications for all feedstock materials that will ensure contribution to the final compact impurities are effectively minimized. For all AGR compact fabrication campaigns, the graphite flake material, resin components, and mold release lubricant were analyzed to ensure low contaminant levels before fabricating the compacts.

Many metals will react with the PyC and SiC layers at fuel operating or accident temperatures to form carbides and/or silicides. Thus, impurities can increase fission product leakage and ultimately result in through-layer failure of the SiC layer or all the TRISO coating layers. The goal of the specified limits on impurities is to verify that impurity levels are sufficiently low as to keep in-pile failures and fission product release below maximum acceptable limits.

The bases for the AGR specifications for compact impurities were evolved from the bases used by GA for DOE HTGR fuel fabrication (Scheffel and Tang 1989; Adams et al. 1992). Early bases reports and fuel specifications often used different units to express the impurity content, including ppm and µg per g burned back particle. Therefore, in utilizing these values as a starting point in developing the AGR specifications (expressed exclusively in µg outside of SiC per compact), conversion was required, taking into account the properties of the particles and compacts (see discussion in Barnes 2006, Appendix B). The limit on Fe impurities in the MHTGR specification was based on the potential for reaction with the SiC layer degrading particle performance. The specification was established based on observed performance in the Fort St. Vrain experience, in which fuel containing approximately 50 µg Fe per g burned back particle exhibited acceptable behavior (Scheffel and Tang 1989). Applied to AGR fuel this results in a corresponding value of ~100 µg per compact and was used to establish the UL_P.

The elements Cr, Mn, Co, and Ni may behave similarly to Fe with respect to attacking the SiC layer. However, the development of the MHTGR and GT-MHR specifications sought to avoid an overly restrictive limit on these elements so that the impurity requirements were consistent with the process capability of the time while still restricting unlimited transition metal contaminations in the compact. In addition, the primary source of these impurities was from steel alloys; therefore, they were controlled indirectly by the Fe specification. This led to a mean specification of ≤55 ppm and an upper limit of ≤1% of compacts exceeding 240 ppm (Munoz 1994; Scheffel and Tang 1989). The AGR fuel specification of ≤50 μg per compact for the mean and an upper limit of ≤1% of compacts exceeding 200 μg per compact are relatively conservative compared to the earlier values.

Limits are placed on concentration of the elements Ti and V because of their ability to catalyze the oxidation of carbonaceous materials (Scheffel and Tang 1989). Early versions of the GA MHTGR fuel specification incorporated a mean value of ≤100 ppm Ti + V, but the specification was subsequently dropped as these elements were included along with a number of other elements in a separate limit imposed on nonburnable boron equivalents that were controlled at a much lower level (Scheffel and Tang 1989). The AGR program converted this specification to a value of ≤400 μg per compact for the AGR-1 fuel specification (Barnes 2006). The value was subsequently revised downward to ≤240 μg per compact in the specifications for AGR-2 and AGR-5/6/7. Limitations on Ca and Al content in the AGR specifications were included based on reactor physics considerations (Petti et al. 2004).

2.6.8 Dispersed Uranium and Compact Defect Fractions

One variable property and two particle defect fractions (attribute properties) are quantified using the deconsolidation-leach-burn-leach (DLBL) method to analyze the fuel compacts. The dispersed uranium fraction (DUF) is a variable property defined as fraction of uranium outside of the SiC layers of the coated particles within the compacts, either in the OPyC layers or the compact matrix, and expressed as the mass of dispersed uranium divided by the total mass of uranium in the compacts. The exposed kernel fraction (EKF) is an attribute property that represents the fraction of particles containing kernels that are not contained by any intact hermetic coating layers so that the fission gas released from the kernel will be readily released from the particle during operation. The SiC defect fraction (SDF) is an attribute property defined as the fraction of particles that have a defective SiC layer that is not retentive of fission products but has at least one intact pyrocarbon so the fission gases would be retained. The nature of these defects and the basis for the values in the fuel specification will be discussed in detail in the subsequent sections. The DLBL process used to quantify these compact properties has been described in detail elsewhere (Hunn et al. 2019) and will be summarized herein.

In the first step of the analysis method, a “clutch” of compacts (typically numbering five in the AGR-5/6/7 analysis) is electrolytically deconsolidated in a process that disintegrates the compact matrix and liberates individual particles. The particles and residual matrix debris are then leached in near-boiling nitric acid in two separate steps. This deconsolidation and preburn leaching will result in the dissolution of a portion of the dispersed uranium and exposed kernels, as defined above. The particle and matrix debris are then heated in air at 750°C to oxidize all exposed carbon, including the matrix debris and the pyrocarbon layers. This results in removal of the OPyC layer on all particles and removal of the IPyC and buffer layers on particles that have a SiC defect. Oxygen will penetrate the SiC through either a gas-permeable defect, such as a crack, or by burning out a carbon pathway, such as may be formed by a carbon soot inclusion or residual carbonaceous material left behind after degradation of the SiC by a silicide forming metal impurity. Subsequent postburn leaching will dissolve any remaining dispersed uranium from the ashed OPyC and matrix debris and from the kernels in particles with SiC defects that have been exposed by the removal of the pyrocarbon layers. Careful analysis of the various leaching solutions for uranium allows these compact properties to be determined, as discussed below.

Dispersed uranium, exposed kernels, and particles with defective SiC exhibit different fission product release behavior during reactor operation. This behavior factors into establishing the corresponding limits

in the specification. Because of the location and fine dispersion of uranium represented by the DUF, it exhibits a relatively high release of fission gases. By comparison, exposed kernels exhibit lower fission gas release because of the larger volume of the kernel and greater diffusion length scale. A particle with defective SiC will be highly retentive of fission gas because at least one pyrocarbon layer remains intact but can exhibit elevated release of certain metallic fission products that would otherwise be well retained by intact SiC (e.g., cesium).

The term "heavy-metal contamination" (HMC) has historically been used in the U.S., including in the AGR-1 and AGR-2 fuel specifications, as the metric for all uranium in a compact that is not encapsulated by a fission gas retentive coating layer. The HMC fraction was based on the uranium mass fraction measured in the deconsolidation and preburn leach acid solutions and, therefore, included both a portion of the dispersed uranium and uranium from exposed kernels.[‡] It was treated as an attribute property for acceptance testing under the assumption that one kernel equivalent of dispersed uranium had the same negative impact as one particle with an exposed kernel defect. The basis for establishing limits on HMC and other defects in fuel specifications for past HTGR development programs, including the U.S. GT-MHR and MHTGR programs, was closely tied to the radionuclide control requirements for the specific reactor and plant design and considerations such as fuel fabrication capabilities.

The AGR-1 fuel specification (Barnes 2006, Appendix A) explains the basis for establishing the property limits for HMC fraction and SDF used at the start of the AGR program. While the historic U.S. TRISO fuel specifications were considered as a starting point, additional considerations factored into the AGR-1 specifications since radionuclide control in an operating HTGR was not a primary concern for in-pile irradiation tests in ATR. These considerations included the following:

1. The quantity of particles needed for destructive examination to verify conformance with the specification. In the case of AGR-1 fuel fabrication, which used a lab-scale (50 mm diameter) coating chamber that produced relatively small batches of coated particles, excessively stringent specifications on these properties would require more coating runs than funding and schedule would allow to produce enough particles for QC while still populating the irradiation capsules.
2. The level of fission gas release from the fuel in an irradiation capsule that could be tolerated while still allowing detection of in-pile failures to achieve the irradiation objectives.
3. Fabrication capabilities were considered, particularly considering the lab-scale process development that went into the AGR-1 fuel fabrication, where the possibility existed that fuel quality would be lower when compared to a mature, large-scale commercial production operation.

The AGR program initially adopted HMC and SDF specifications for AGR-1. The values, while established based on the historic GT-MHR specifications, were slightly less stringent based on the considerations enumerated above (HMC fraction $\leq 1\times10^{-4}$ and SDF $\leq 2\times10^{-4}$; Barnes 2006). These were revised downward for the AGR-2 specification (Barnes 2009) to $\leq 2\times10^{-5}$ for HMC and $\leq 1\times10^{-4}$ for SDF, which is consistent with the GT-MHR fuel specification for the compact lots (Munoz 1994).

The program subsequently elected to separate the HMC specification into DUF and EKF. This allowed separate values to be set for each property considering the different level of fission gas release from each source of uranium in the fuel and provided greater feedback on the sources of uncontained uranium. This change was also prompted by the fact that not all dispersed uranium is collected during the preburn leach step; therefore, improved values can be obtained by judicious use of postburn leach data, as described in the following sections. The final AGR-5/6/7 fuel specification limiting DUF to $\leq 1\times10^{-5}$ and EKF to $\leq 5\times10^{-5}$ reflects the lower fission gas release from exposed kernels. The SDF fraction was unchanged from AGR-2 at $\leq 1\times10^{-4}$. For AGR-5/6/7, DUF, EKF, and SDF were only specified for the

[‡] In the German fuel development program, heavy metal contamination in the fuel pebbles was determined using a burn-leach procedure, which would simultaneously dissolve and quantify dispersed uranium, exposed kernels, and kernels of particles with SiC defects. This program did not differentiate between exposed kernels and SiC defects as discussed in this report.

compact lot. However, the same analysis (except for the compact deconsolidation step) was applied to the coated particles, with the data gathered for information only. This provided a baseline for feedback on the compacting process and allowed for proactive selection of coated particle lots to be used in compacting (Marshall 2020).

2.6.8.1 Dispersed Uranium Fraction

Dispersed uranium may be caused by uranium fines originating from the abrasion of fuel kernels after they are charged to the coater vessel and before a protective buffer layer is sufficiently deposited to protect the kernels. This uranium may be dispersed throughout the particle coatings but is quantified for the purpose of measuring DUF only from deposits on the surface of the SiC layer and embedded within the OPyC layer as these are locations that lead to fission product release. Another source of dispersed uranium is the trace uranium naturally present in the graphite powders and other constituents used to formulate the compact matrix. Uranium contamination in coated particles or compacts can also be picked up from residual uranium contamination in the coating furnace or furnaces used for compact heat treatment. All these sources of uranium contamination can increase the average dispersed uranium content and result in elevated levels of uncontained fission products that can be released into the fuel body and reactor coolant during operation.

The DUF is measured by the background levels of uranium recovered during the preburn and postburn leaches of the compact DLBL process only if no exposed kernels or SiC defects are present that would permit the dissolution of a kernel contributing to the total recovered uranium. The preburn leach recovers some of the dispersed uranium in the deconsolidated compact matrix, on the coated particle surface, and in the outer few microns of the OPyC layer. Following the burn back of the OPyC layer, the ash and SiC surface are leached to recover the remainder of the dispersed uranium. For clutches exhibiting no exposed kernels or SiC defects, the total DUF is taken as the sum of preburn and postburn dispersed uranium fractions. The fact that dispersed uranium is not fully quantified until the burn-leach phase of the DLBL procedure was one of the motivations for bifurcating the HMC specification into DUF and EKF.

For clutches of compacts containing one or more exposed kernel or SiC defect, the quantity of recovered uranium is typically near the level that is equivalent to an integer multiple of a fuel kernel inventory because uranium from the dissolved kernels dominates the total measured value. For these clutches, the data are evaluated to determine the number of particle defects present. For the AGR-5/6/7 fuel QC analyses, those clutches having less than half of a kernel equivalent were treated as having no particle defects based on the assumption that only dispersed uranium contributed to the total recovered uranium. Clutches exhibiting greater than 50% of a kernel inventory in the preburn leaches were treated as manifesting exposed kernels, and those with greater than 50% of a kernel inventory in the postburn leaches were treated as manifesting defective SiC. In practice, the uranium level used to discriminate between dispersed uranium and dissolved kernels can be specified as appropriate given the nature and level of dispersed uranium.

To take advantage of the higher allowable limit for EKF and SDF, it is important to be able to discriminate between the leached uranium from dispersed uranium and from particles with exposed kernels or SiC defects. Otherwise, the conservative approach would be to assume all the leached uranium originates from the most stringent criteria (i.e., the DUF). Using the DLBL process to differentiate between dispersed uranium and particle defects requires that the level of dispersed uranium in a clutch be significantly less than a single kernel equivalent and that some measured clutches do not have defective particles. If the average amount of dispersed uranium in a clutch is close to the discrimination limit between dispersed uranium and defective particles (e.g., 0.5 for AGR-5/6/7), it will be difficult to discern whether the uranium source in the leach solutions is from dispersed uranium or the dissolved kernels of defective particles. In this case, the number of fuel elements in a clutch must be reduced to provide more discrimination between dispersed uranium and dissolved kernels. If clutch size is reduced to the smallest

integral of one fuel element per clutch and the DLBL of single fuel elements still yields more than the discrimination limit for every measured fuel element, it is likely that the lot will fail to satisfy the specification regardless of whether the leached uranium is counted toward the DUF, EKF, or SDF. For the AGR-5/6/7 fuel, a typical clutch of five compacts with no particle defects had dispersed uranium equivalent to a few percent of one kernel inventory (Hunn et al. 2019). This confirmed that the combined analysis of five AGR-5/6/7 compacts per clutch was appropriate and suggested that a lower threshold could have been used to discriminate between dispersed uranium and dissolved kernels to ensure partially leached kernels in defective particles were not counted in the DUF but were rather appropriately counted as defective particles.

2.6.8.2 Exposed Kernel Fraction

Exposed kernels have no hermetic coating layers intact to retain fission gas. The specification for the allowable maximum EKF is applied to the final fuel form. However, the EKF is often also measured on coated particle lots for information only. In this way, significant change in the EKF assessed for compacts gauges whether particle damage occurred during the particle overcoating or compact formation stages. Measurement of the preburn and postburn uranium faction in coated particle lots was required in the AGR-5/6/7 fuel specification for information only to assess whether the particle population used for compacting exhibited excessively high fraction of defects associated with the coating process and coated particle handling prior to overcoating and compacting.

For the AGR-5/6/7 fuel characterization, preburn leaches recovering more than 50% of a fuel kernel equivalent from a clutch of compacts were treated as having exposed kernels, and the rounded integer number of leached kernel equivalents was used to enumerate the number of particles with an exposed kernel defect to perform acceptance testing of the EKF as an attribute property. The leached kernel equivalents are expected to typically be within 10–20% of an integral value for TRISO fuel with appropriately tight tolerances on uranium loading in the kernels and a sufficient DLBL procedure. The reasons for recovering values deviating significantly from an integer multiple of a kernel equivalent include (1) the uranium content of an exposed kernel was significantly above or below average (such as would be observed for significantly undersized and oversized kernels or if the exposed kernel was missing a fragment) or (2) the LBL process itself was incomplete, which could be related to coating layer cracks so small that the acid could not fully dissolve the kernel or to inappropriate leach times (this can be mitigated by performing successive leaches to evaluate if leaching is complete). Sampled clutches with a large number of defects may also have cumulative deviations that combine to produce a larger offset from an integer value. In addition to these possibilities, a portion of the DUF is recovered simultaneously and is indistinguishable from the dissolved kernels. It is not uncommon for the recovered kernel equivalents to exceed integer values by an amount of equivalent magnitude to the preburn DUF.

The EKF metric is sensitive to any mechanical damage to the TRISO particles during handling and compaction. A significant increase in the EKF in compacted vs. uncompacted AGR-5/6/7 coated particles indicated that the compaction process for AGR-5/6/7 had caused particle damage in compacts with a ~40% particle packing fraction (Marshall 2020). This was likely due to a combination of the high particle packing fraction (the effect was not observed with the nominally 25% packing fraction compacts), the high matrix density, and the compaction method. Particle damage was not observed following compacting of the AGR-1 (up to 37.4% packing fraction) or AGR-2 (36.8% packing fraction) coated particles (Phillips, Barnes, and Hunn 2010).

2.6.8.3 SiC Defect Fraction

Fission product release through a defective SiC layer is less than that associated with exposed kernels or dispersed uranium, which supports the higher limit on this defect fraction in the fuel specification. Particles with SiC defects and at least one intact PyC layer will effectively retain gaseous fission products, while releasing other fission products (e.g., cesium) that can readily diffuse through carbonaceous material. A defective SiC layer may still attenuate the migration of fission products. Defective SiC particles with broken or missing SiC layers will have a higher release-to-birth ratio than those with solid carbonaceous pathways through the SiC, but the DLBL analysis method does not distinguish between these different types of SiC defects.

Like the EKF, the SDF was quantified from leached AGR-5/6/7 compact clutches in which more than one-half of a kernel equivalent of uranium was dissolved, except that data was collected from the postburn leaches after the burn step had removed the intact pyrocarbon layer(s) that prevented kernel leaching during the preburn leaches. The SDF is also sensitive to incomplete leaching. The reasons for recovering values deviating significantly from an integer multiple of a kernel equivalent stem from the same factors that can impact the EKF and from incompletely leached particles with exposed kernel defects and inadequate burning of the exposed carbonaceous material. The effectiveness of the burn phase is impacted by allowing sufficient time for gas transport to and from the kernel. Very small SiC defects may require several days of heating in air at temperatures from 750°C to 850°C to fully oxidize the IPyC and buffer layers. A 72-hour burn step was used for the AGR-5/6/7 fuel particles (Hunn et al. 2019).

2.6.8.4 Defective OPyC Fraction

An OPyC defect fraction limit is applied in the compact specification that is distinct from that applied to the coated particles (see discussion in Section 2.5.7). This is used to assess the level of OPyC damage that may have occurred during compact formation and provide the total level of defects in the final fuel compact. The specified limit established in the AGR program ($\leq$0.01) is higher than the specification for the coated particle lots (see Table 5), which allows for additional defect formation during compact fabrication and is consistent with the prior GT-MHR specification (Munoz 1994). The relatively high value compared to other particle defect specifications reflects the lower impact that a defective OPyC layer has on fission product retention (since the IPyC and SiC layers still perform this function) and on coated particle failure probability (Scheffel and Tang 1989).

3. CONCLUSIONS

This report describes the technical bases for the AGR-5/6/7 reference TRISO fuel specification. The importance of each kernel, coated particle, and compact property in the specification as it relates to fuel performance is discussed. The impact on the performance of fuel failing to meet the specification values is also presented.

The report often relates the AGR values to specifications established during earlier U.S. TRISO fuel development programs, including the GT-MHR and MHTGR fuel product specifications (Tang 1989; Munoz 1994) and the specifications established early in the AGR program. The starting point for many of the AGR program specifications was the previous U.S. HTGR programs that needed to consider radionuclide control with a reactor system and power plant as part of a comprehensive safety analysis. While preserving many of the previously established values, evolution of AGR program fuel specifications reflected the needs of a fuel qualification program performing irradiation experiments in a materials test reactor and the progress in the development of fuel fabrication and characterization capabilities.

In some instances, fuel characterization methods were developed or improved during the AGR program to enable quantification of properties not traditionally examined for TRISO fuel populations and not included in the fuel specification. Examples include the quantification of particle-to-particle variations

in UCO kernel oxide and carbide phase composition, identification of maximum localized curvature in kernels and coatings, and various X-ray tomography techniques that provide detailed information about abnormal coating microstructure and offer alternate methods for nondestructive characterization of final fuel forms. These innovations could be applied to future coated particle fuel development efforts to better characterize particle properties and property distributions and further advance the knowledge of TRISO fuel performance in the technical community.

The goal of TRISO fuel specifications is to constrain the properties well within ranges that will result in acceptable fuel performance. These restrict the number of particles that exceed critical limits where performance begins to noticeably degrade to very low fractions, such that the impact on overall particle failure fractions remains low. Ultimately, well designed and optimized processes should not require the use of fuel at the boundary of the performance limit in order to increase yield. It is better for a manufacturer to expend effort in optimizing the process to hit the center of the design space than to perform extensive tests to qualify fuel produced using a poorly controlled process.

4. REFERENCES

Adams, C. C., D. G. Czechowicz, S. P. Munoz, and C. A. Stone. 1992. "NP-MHTGR Fuel Product Specification Basis Report." CEGA-000396, Rev. 0, CEGA Corp.

Bacon, G. E. 1956. "A Method for Determining the Degree of Orientation of Graphite." Journal of Applied Chemistry 6(11): 477–481.

Barnes, C.M. 2005. "AGR-1 Fuel Product Specification and Characterization Guidance." EDF-4380, Rev. 2, Idaho National Laboratory.

Barnes, C. M. 2006. "AGR-1 Fuel Product Specification and Characterization Guidance." EDF-4380, Rev. 8, Idaho National Laboratory.

Barnes, C. M., W. C. Richardson, D. L. Husser, and M. A. Ebner. 2008. "Fabrication Process and Product Quality Improvements in Advanced Gas Reactor UCO Kernels." Proceedings of the 4th International Topical Meeting on High Temperature Reactor Technology (HTR-2008). Washington D.C., September 28–October 1, 2008. https://inldigitallibrary.inl.gov/sites/sti/sti/4074959.pdf

Barnes, C. M. 2009. "AGR-2 Fuel Specification." SPC-923, Rev. 3, Idaho National Laboratory.

Barnes, C. M., and D. W. Marshall. 2009. "FY 2009 Particle Fabrication and Coater Test Report." INL/EXT-09-16545, Idaho National Laboratory.

Bower, G. R., S. A. Ploger, P. A. Demkowicz, J. D. Hunn. 2017. "Measurement of Kernel Swelling and Buffer Densification in Irradiated UCO-TRISO Particles." Journal of Nuclear Materials 486: 339–349.

Bresnik, S. 1991. "MHTGR Fuel Process and Quality Control Description." DOE-HTGR-90257 Rev. 0, General Atomics. https://www.nrc.gov/docs/ML0302/ML030230825.pdf

Bullock, R. E. 1984. "Fission-Product Release during Post-Irradiation Annealing of Several Types of Coated Fuel particles." Journal of Nuclear Materials 125: 304–319.

Bullock, R. E., and C. Young. 1994. "TRISO Fuel Particle Design Basis." DOE-GT-MHR100225, General Atomics.

Collin, B. P. 2018a. "AGR-2 Irradiation Experiment Test Plan." PLN-3798, Rev. 2, Idaho National Laboratory.

Collin, B. P. 2018b. "AGR-5/6/7 Irradiation Experiment Test Plan." PLN-5245, Rev. 1, Idaho National Laboratory.

Demkowicz, P. A., J. D. Hunn, R. N. Morris, I. J. van Rooyen, T. J. Gerczak, J. M. Harp, and S. A. Ploger. 2015. "AGR-1 Post Irradiation Examination Final Report." INL/EXT-15-36407. Idaho National Laboratory.

Demkowicz, P. A., J. D. Hunn, D. A. Petti, and R. N. Morris. 2018. "Key Results from Irradiation and Post-irradiation Examination of AGR-1 UCO TRISO Fuel." Nuclear Engineering and Design 329: 102–109. https://doi.org/10.1016/j.nucengdes.2017.09.005

Ebner, M. A. 2004. "Chemistry Improvement for the Production of LEU UCO Fuel Using Manufacturing Scale Equipment—FY 2004 Final Report." INL/EXT-04-02372, Idaho National Laboratory.

Ebner, M. A. 2005. "Chemistry Improvement Tests for the Production of LEU UCO Fuel Using Manufacturing Scale Equipment FY 2005 Final Report." INL/EXT-05-00618, Idaho National Laboratory.

Einerson, J. J. 2005. "Statistical Methods Handbook for Advanced Gas Reactor Fuel Materials." INL/EXT-05-00349, Idaho National Laboratory.

Einerson, J. J. 2016. "Statistical Sampling Plan for AGR-5/6/7 Fuel Materials." PLN-4352, Rev. 5, INL/MIS-12-26856, Idaho National Laboratory.

Federer, J. I. 1977. "Fluidized Bed Deposition and Evaluation of Silicon Carbide Coatings on Microspheres." ORNL/TM-5152, Oak Ridge National Laboratory.

General Atomics. 2009. "Final Report – NGNP Core Performance Analysis, Phase 2." 91184.

General Atomics. 2010. "Conceptual Design Summary Report – Steam Cycle Modular Helium Reactor Plant." NGNP-R00016, Rev. 0.

Goodin, D. T., M. J. Kania, and B. W. Patton. 1989. "Experimental Plan for Irradiation Experiment HRB-21." DOE-HTGR-87-091, Oak Ridge National Laboratory.

Hanke, H. J. 1992. "Performance of High Quality HTR-LEU-Fuel Elements with TRISO Coated Particles, Summary Report." KFA-HTA-IB-7/92, Forschunstrum Jülich GmbH.

Hanson, D. L. 2001. "Logic for Deriving Quality Specifications." PC-000498/0, General Atomics.

Hanson, D. L. 2009. "Technical Basis for NGNP Fuel Performance and Quality Requirements." GA-911168/0, General Atomics. https://art.inl.gov/NGNP/Subcontractors Documents/General Atomics/Technical Basis for NGNP Fuel Performance and Quality Requirements.pdf

Hantke, H. J. 1992. "Performance of High Quality HTR-LEU-Fuel Elements with TRISO Coated Particles." HTA-IB-7/92, Forschungszentrum Jülich GmbH.

Heit, W., H. Huschka, W. Rind, G. G. Kaiser. 1985. "Status of Qualification of High-temperature Reactor Fuel Elements Spheres." Nuclear Technology 69: 44–54.

Helmreich, G. W., J. D. Hunn, D. J. Skitt, J. A. Dyer, A. T. Schumacher. 2017. "Acceptance Test Data for the AGR-5/6/7 Irradiation Test Fuel TRISO Composite." ORNL/TM-2017/037, Oak Ridge National Laboratory.

Helmreich, G. W., J. D. Hunn, J. W. McMurray, and D. R. Brown. 2020a. "Enhanced Method for Analysis of Individual UCO Kernel Phase Fractions." Nuclear Engineering and Design 363: 110625.

Helmreich, G. W., D. R. Brown, T. J. Gerczak, J. D. Hunn. 2020b. "Quantification of Silicon Carbide Grain Structure in TRISO Fuel by BSE Image Analysis." Journal of Nuclear Materials 533: 152075.

Homan, F. J., T. B. Lindemer, E. L. Long Jr., T. N. Tiegs, and R. L. Beatty. 1977. "Stoichiometric Effects on Performance of High-Temperature Gas-Cooled Reactor Fuel from the U-C-O System." Nuclear Technology 35(2): 428–441.

Hunn, J. D. 2004a. “Results from ORNL Characterization of Nominal 350 µm NUCO Kernels from the BWXT 69300 Composite.” ORNL/TM-2005/545, Oak Ridge National Laboratory.

Hunn, J. D. 2004b. “Results from ORNL Characterization of German Reference Fuel from EUO 2358–2365 Composite.” ORNL/TM-2005/546, Oak Ridge National Laboratory.

Hunn, J. D., A. K. Kercher, P. A. Menchhofer, and J. R. Price. 2005. “Results from ORNL Characterization of Nominal 350 µm NUCO Kernels from the BWXT 59344 Batch.” ORNL/TM-2005/541, Oak Ridge National Laboratory.

Hunn, J. D. 2005. “Data Acquisition Method for Measurement of Pyrocarbon Anisotropy using the Two-Modulator Generalized Ellipsometry Microscope (2-MGEM).” AGR-CHAR-DAM-18, Rev. 1, Oak Ridge National Laboratory.

Hunn, J. D. 2006. “Data Acquisition Method for Measurement of Buffer Envelope Density using a Mercury Porosimeter.” AGR-CHAR-DAM-16, Rev. 3, Oak Ridge National Laboratory.

Hunn, J. D., and R. A. Lowden. 2006. “Data Compilation for AGR-1 Variant 3 Coated Particle Composite LEU01-49T.” ORNL/TM-2006/022, Oak Ridge National Laboratory.

Hunn, J. D. 2008. “Data Acquisition Method for Counting of Particles with SiC Soot Inclusion Defects by Visual Inspection.” AGR-CHAR-DAM-32, Rev. 0, Oak Ridge National Laboratory.

Hunn, J. D., G. E. Jellison Jr., and R. A. Lowden. 2008. “Increase in Pyrolytic Carbon Optical Anisotropy and Density During Processing of Coated Particle Fuel Due to Heat Treatment.” Journal of Nuclear Materials 374(3): 445–452.

Hunn, J. D., T. W. Savage, and C. M. Silva. 2010. “AGR-2 Fuel Compact Pre-Irradiation Characterization Summary Report.” ORNL/TM-2010/226. Oak Ridge National Laboratory.

Hunn, J. D., T. W. Savage, and C. M. Silva. 2012. “AGR-1 Fuel Compact Pre-Irradiation Characterization Summary Report.” ORNL/TM-2012/295. Oak Ridge National Laboratory.

Hunn, J. D. 2013. “Data Acquisition Method for Imaging of SiC Grain Structure.” AGR-CHAR-DAM-23, Rev. 1, Oak Ridge National Laboratory.

Hunn, J. D., R. N. Morris, C. A. Baldwin, F. C. Montgomery, C. M. Silva, and T. J. Gerczak. 2013. “PIE on Three Irradiated AGR-1 Compacts in FY2013.” ORNL/LTR-2013/291, Oak Ridge National Laboratory.

Hunn, J. D., C. A. Baldwin, T. J. Gerczak, F. C. Montgomery, R. N. Morris, M.C. Silva, P. A. Demkowicz, J. M. Harp, S. A. Ploger, I. van Rooyen, and K. E. Wright. 2014. “Detection and Analysis of Particles with Failed SiC in AGR-1 Fuel Compacts.” Proceedings of the 7th International Topical Meeting on High Temperature Reactor Technology (HTR-2014). Weihai, October 27–31, 2014. Also published in Nuclear Engineering and Design 306: 36–46.

Hunn, J. D., R. N. Morris, C. A. Baldwin, F. C. Montgomery, and T. J. Gerczak. 2015. “PIE on Safety-Tested AGR-1 Compact 5-1-1.” ORNL/TM-2015/317, Oak Ridge National Laboratory.

Hunn, J. D., F. C. Montgomery, G. W. Helmreich, and A. K. Kercher. 2019. “Additional Confirmatory LBL Analysis of AGR-5/6/7 Compacts and Overcoated Particles.” ORNL/TM-2019/1154, Oak Ridge National Laboratory.

Jellison, G. E. Jr., J. D. Hunn, and R. A. Lowden. 2006. “Optical Characterization of Tristructural Isotropic Fuel Particle Cross-sections Using Generalized Ellipsometry.” Journal of Nuclear Materials 352: 6–12.

Jellison, G. E. Jr., and J. D. Hunn. 2008, “Optical Anisotropy Measurements of TRISO Nuclear Fuel Particle Cross Sections: The Method.” Journal of Nuclear Materials 372: 36–44.

Jellison, G. E. Jr., J.D. Hunn, F. Charollais, H. Rouquette, O. Dugne. 2010. "Comparison of Optical Characterization Methods for Anisotropy of TRISO Particle Layers." INERI Project 2006-003-F Final Report, ORNL/TM-2010/003, Oak Ridge National Laboratory.

Kania, M. J., H. Nabielek, K. Verfondern, H. J. Allelein. 2013. "Testing of HTR UO_2 TRISO Fuels in AVR and in Material Test Reactors." J. of Nuclear Materials 441: 545–562.

Kercher, A. K., and J. D. Hunn. 2005a. "Statistical Methods for Material Characterization and Qualification." ORNL/TM-2005/542, Oak Ridge National Laboratory.

Kercher, A. K., and J. D. Hunn. 2005b. "Results from ORNL Characterization of Nominal 350 μm LEUCO Kernels from the BWXT G73D-20-69302 Composite." ORNL/TM-2005/517, Oak Ridge National Laboratory.

Kercher, A. K., and J. D. Hunn. 2006. "Results from ORNL Characterization of Nominal 350 μm LEUCO Kernels (LEU03) from the BWXT G73D-20-69303 Composite." ORNL/TM-2006/552, Oak Ridge National Laboratory.

Kugeler, K. N. 2017. "The High Temperature Gas-cooled Reactor, Safety considerations of the (V)HTR-Modul." EUR 28712 EN, European Commission, DG Joint Research Centre. https://doi.org/10.2760/270321

Lowden, R. A., J. D. Hunn, S. D. Nunn, A. K. Kercher, J. R. Price, P. A. Menchhifer, and G. E. Jellison Jr. 2005. "Effects of Deposition Conditions on the Properties of Pyrolytic Carbon Deposited in a Fluidized Bed." ORNL/TM-2005/533, Oak Ridge National Laboratory.

Lowden, R. A. 2006. "Fabrication of Baseline and Variant Particle Fuel for AGR-1." ORNL/CF-06/02, Oak Ridge National Laboratory.

Maki, J. T., D. A. Petti, R. R. Hobbins, R. K. McCardell, E. L. Shaber, and F. H. Southworth. 2002. "NP-MHTGR Fuel Development Program Results." INEEL/EXT-02-01268, Idaho National Laboratory.

Maki, J. T., D. A. Petti, D. L. Knudson, and G. K. Miller. 2007. "The Challenges Associated with High Burnup, High Temperature, and Accelerated Irradiation for TRISO-Coated Particle Fuel." Journal of Nuclear Materials 371: 270–280. https://doi.org/10.1016/j.jnucmat.2007.05.019

Marshall, D. M. 2012. "TRISO Particle Coating Development Status." Presentation at the AGR Program Technical Coordination Team meeting held on Feb. 28–Mar. 1, 2012, San Diego, CA.

Marshall, D. M. 2017. "AGR-5/6/7 Fuel Specification." SPC-1352, Rev. 8, INL/MIS-11-21423. Idaho National Laboratory.

Marshall, D. M. 2020. "AGR-5/6/7 Fuel Fabrication Report." INL/EXT-19-53720, Rev. 1, Idaho National Laboratory.

McMurray, J. W., T. B. Lindemer, N. R. Brown, T. J. Reif, R. N. Morris, and J. D. Hunn. 2017. "Determining the Minimum Required Uranium Carbide Content for HTGR UCO Fuel Kernels." Annals of Nuclear Energy 104: 237–242.

Miller, G. K., and D. C. Wadsworth. 1994. "Treating Asphericity in Fuel Particle Pressure Vessel Modeling." Journal of Nuclear Materials 211(1): 57–69.

Miller, G. K., D. A. Petti, and J. T. Maki. 2004. "Consideration of the Effects of Partial Debonding of the IPyC and Particle Asphericity on TRISO-coated Fuel Behavior." Journal of Nuclear Materials 33: 79–89.

Morris, R. N., C. A. Baldwin, P. A. Demkowicz, J. D. Hunn, and E. L. Reber. 2014. "Performance of AGR-1 High-Temperature Reactor Fuel During Post-Irradiation Heating Tests." Proceedings of the

7th International Topical Meeting on High Temperature Reactor Technology (HTR-2014). Weihai, October 27–31, 2014. Also published in Nuclear Engineering and Design 360: 24–35.

Munoz, S. P. 1994. "Fuel Product Specification." DOE-GT-MHR-100209, General Atomics.

Petti, D. A., J. T. Maki, J. Buongiorno, R. R. Hobbins, and G. K. Miller. 2002. "Key Differences in the Fabrication, Irradiation and Safety Testing of U.S. and German TRISO-Coated Particle Fuel and their Implications on Fuel Performance." INEEL/EXT-02-00300, Idaho National Laboratory.

Petti, D. A., J. T. Maki, M. A. Ebner, and G. K. Miller. 2004. "Preliminary AGR Fuel Specification." EDF-4198, Rev. 1, Idaho National Laboratory.

Petti, D. A., J. T. Maki, J. D. Hunn, P. J. Pappano, C. M. Barnes, J. J. Saurwein, S. G. Nagley, J. M. Kendall, and R. R. Hobbins. 2010. "The DOE Advanced Gas Reactor Fuel Development and Qualification Program." JOM 62(9): 62–66.

Pham, B. T., J. J. Palmer, D. W. Marshall, J. W. Sterbentz, G. L. Hawkes, and D. M. Scates. 2021. "AGR-5/6/7 Irradiation Test Final As-Run Report." INL/EXT-21-64221, Idaho National Laboratory.

Phillips, J. A., C. M. Barnes, and J. D. Hunn. 2010. "Fabrication and Comparison of Fuels for Advanced Gas Reactor Irradiation Tests." Paper 236 in Proceedings of the 5th International Topical Meeting on High Temperature Reactor Technology (HTR-2010), Prague, October 18–20, 2010.

Phillips, J. A., E. L. Shaber, J. J. Einerson, D. A. Petti, S. E. Niedzialek, W. C. Richardson, S. G. Nagley. 2012. "Compacting scale up and optimization of cylindrical fuel compacts for the Next Generation Nuclear Plant." HTR2012-3-001, Proceedings of the 6th International Topical Meeting on High Temperature Reactor Technology (HTR2012), Tokyo, Japan, October 28–November 1, 2012.

Ploger, S. A., P. A. Demkowicz, J. D. Hunn, J. S. Kehn. 2012. "Ceramographic Examinations of Irradiated AGR-1 Fuel Compacts." INL/EXT-12–25301, Rev. 1, Idaho National Laboratory.

Ploger, S. A., P. A. Demkowicz, J. D. Hunn, and J. S. Kehn. 2014. "Microscopic Analysis of Irradiated AGR-1 Fuel Compacts." Nuclear Engineering and Design 271: 221–230.

Pointud, M. L., and P. Chenebault. 1977. "Emission of Fission Gases by Failed Coated Oxide Fuel Particles." Nuclear Technology 35(2): 494–500.

Price, R. J. 1977. "Properties of Silicon Carbide for Nuclear Fuel Particle Coatings." Nuclear Technology 35(2): 320–336. https://doi.org/10.13182/NT77-A31892

Price, J. R., D. B. Aykac, J. D. Hunn, A. K. Kercher, and R. N. Morris. 2006. "New Developments in Image-based Characterization of Coated Particle Nuclear Fuel." Proceedings of Machine Vision Applications in Industrial Inspection XIV, SPIE 6070: 153–162.

Saurwein, J. J. 1995. "Acceptance Test Report for German Fuel Particles." GA-910852, General Atomics.

Scheffel, W. J., and I. M. Tang. 1989. "Technical Support Document of the MHTGR Fuel Product Specification." GA-903728, General Atomics.

Scheffel, W. J., D. T. Goodin, I. M. Tang, and C. A. Young. 1991. "Capsule HRB-21 Pre-Irradiation Report." DOE-HTGR-88357, General Atomics.

Scheffel, W. J., and J. J. Saurwein. 2002. "Preliminary Fuel Product Specification for the Baseline Advanced Gas Reactor Fuel Design." GA-911034, General Atomics.

Skerjanc, W. F. 2013. "Fuel Performance Basis for AGR-5/6/7 Fuel Specification Using PARFUME." ECAR-2341, Idaho National Laboratory.

Skerjanc, W. F., J. T. Maki, B. P. Collin, and D. A. Petti. 2016. "Evaluation of Design Parameters for TRISO-coated Fuel Particles to Establish Manufacturing Critical Limits Using PARFUME." J. of Nuclear Materials 469: 99–105. https://doi.org/10.1016/j.jnucmat.2015.11.027

Snead, L. L., T. Nozawa, Y. Katoh, T. S. Byun, S. Kondo, and D. A. Petti. 2007. "Handbook of SiC Properties for Fuel Performance Modeling." Journal of Nuclear Materials 371: 329–377.

Stempien, J. D., J. D. Hunn, R. N. Morris, T. J. Gerczak, and P. A. Demkowicz. 2021. "AGR-2 TRISO Fuel Post-Irradiation Examination Final Report." INL/EXT-21-64279. Idaho National Laboratory.

Stevens, D. W. 1979. "Round Robin Optical Menasurements of Preferred Orientation in Nearly Isotropic Pyrocarbon." GA-A15291, General Atomics.

Tang, I. M. 1989. "MHTGR Fuel Product Specification." DOE-HTGR-88140, General Atomics.

Technical Coordination Team (TCT). 2012. "Summary of the Advanced Gas Reactor Fuel Development and Qualification Program Technical Coordination Team Meeting." October 23–24, 2012, Park City, UT.

Verfondern, K., H. Nabielek, and J. M. Kendall. 2007. "Coated Particle Fuel for High Temperature Gas Cooled Reactors." Nuclear Engineering and Technology 39(5): 603–616. https://doi.org/10.5516/NET.2007.39.5.603